Article

Cell Host & Microbe

Induction of alarmin S100A8/A9 mediates activation of aberrant neutrophils in the pathogenesis of COVID-19

Graphical abstract

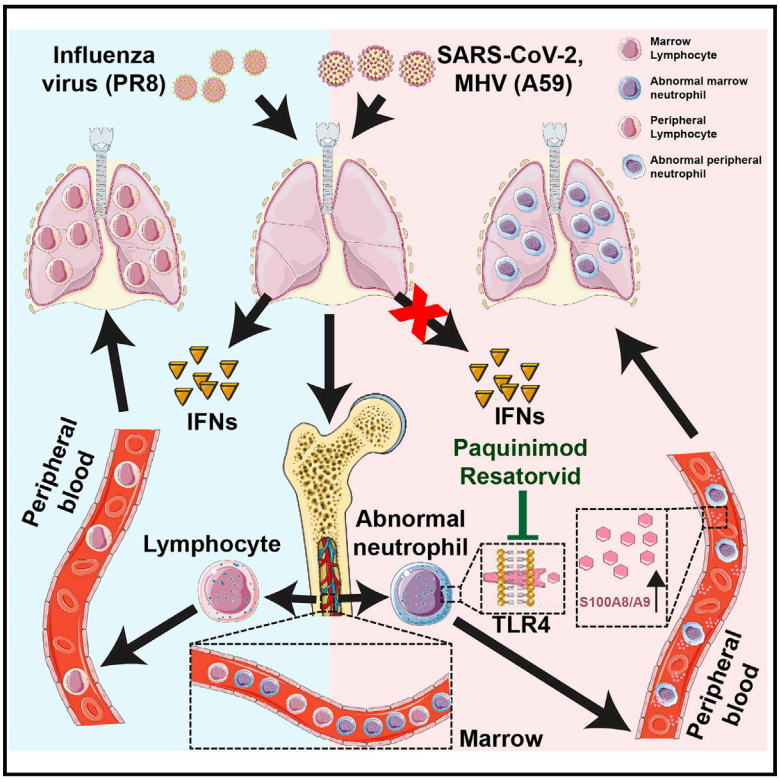

Highlights

- S100A8 is dramatically upregulated in SARS-CoV-2-infected animal models and patients
- A group of aberrant immature neutrophils is induced during SARS-CoV-2 infection
- Immune disorder is mediated by the S100A8/A9-TLR4 pathway
- S100A8/A9 inhibitor, Paquinimod, could prevent COVID-19-associated immune disorder

Authors

Qirui Guo, Yingchi Zhao, Junhong Li, ..., Chuan Qin, Xiangxi Wang, Fuping You

Correspondence

qinchuan@pumc.edu.cn (C.Q.), xiangxi@ibp.ac.cn (X.W.), fupingyou@hsc.pku.edu.cn (F.Y.)

In Brief

Guo et al. demonstrate that over-activation of S100A8/A9-TLR4 signaling results in immune imbalance and expansion of aberrant immature neutrophils during SARS-CoV-2 infection. Relevant therapeutic targets were validated in animal infection models.

Guo et al., 2021, Cell Host & Microbe *29*, 222–235
February 10, 2021
https://doi.org/10.1016/j.chom.2020.12.016

CellPress

CellPress
OPEN ACCESS

Cell Host & Microbe

Article

Induction of alarmin S100A8/A9 mediates activation of aberrant neutrophils in the pathogenesis of COVID-19

Qirui Guo,[1,4] Yingchi Zhao,[1,4] Junhong Li,[2,4] Jiangning Liu,[3,4] Xiuhong Yang,[3,4] Xuefei Guo,[1] Ming Kuang,[1] Huawei Xia,[1] Zeming Zhang,[1] Lili Cao,[1] Yujie Luo,[1] Linlin Bao,[3] Xiao Wang,[1] Xuemei Wei,[1] Wei Deng,[3] Nan Wang,[2] Luoying Chen,[1] Jingxuan Chen,[1] Hua Zhu,[3] Ran Gao,[3] Chuan Qin,[3,*] Xiangxi Wang,[2,*] and Fuping You[1,5,*]

[1]Institute of Systems Biomedicine, Department of Immunology, School of Basic Medical Sciences, Beijing Key Laboratory of Tumor Systems Biology, Peking University Health Science Center, Beijing, China

[2]University of Chinese Academy of Sciences, CAS Key Laboratory of Infection and Immunity, National Laboratory of Macromolecules, Institute of Biophysics, Chinese Academy of Sciences, Beijing, China

[3]Key Laboratory of Human Disease Comparative Medicine, Chinese Ministry of Health, Beijing Key Laboratory for Animal Models of Emerging and Remerging Infectious Diseases, Institute of Laboratory Animal Science, Chinese Academy of Medical Sciences and Comparative Medicine Center, Peking Union Medical College, Beijing, China

[4]These authors contributed equally to this work

[5]Lead contact

*Correspondence: qinchuan@pumc.edu.cn (C.Q.), xiangxi@ibp.ac.cn (X.W.), fupingyou@hsc.pku.edu.cn (F.Y.)

https://doi.org/10.1016/j.chom.2020.12.016

SUMMARY

The severe acute respiratory syndrome coronavirus 2 (SARS-CoV-2) pandemic poses an unprecedented public health crisis. Evidence suggests that SARS-CoV-2 infection causes dysregulation of the immune system. However, the unique signature of early immune responses remains elusive. We characterized the transcriptome of rhesus macaques and mice infected with SARS-CoV-2. Alarmin S100A8 was robustly induced in SARS-CoV-2-infected animal models as well as in COVID-19 patients. Paquinimod, a specific inhibitor of S100A8/A9, could rescue the pneumonia with substantial reduction of viral loads in SARS-CoV-2-infected mice. Remarkably, Paquinimod treatment resulted in almost 100% survival in a lethal model of mouse coronavirus infection using the mouse hepatitis virus (MHV). A group of neutrophils that contributes to the uncontrolled pathological damage and onset of COVID-19 was dramatically induced by coronavirus infection. Paquinimod treatment could reduce these neutrophils and regain anti-viral responses, unveiling key roles of S100A8/A9 and aberrant neutrophils in the pathogenesis of COVID-19, highlighting new opportunities for therapeutic intervention.

INTRODUCTION

The ongoing coronavirus disease 2019 (COVID-19) caused by severe acute respiratory syndrome coronavirus 2 (SARS-CoV-2) has resulted in an unprecedented public health crisis, requiring a deep understanding of the pathogenesis and developments of effective COVID-19 therapeutics (Wu et al., 2020b; Zhu et al., 2020). Innate immunity is an important arm of the mammalian immune system, which serves as the first line of host defense against pathogens. Most of the cells of the body harbor the protective machinery of the innate immunity and can recognize foreign invading viruses (Akira et al., 2006). The innate immune system recognizes microorganisms via pattern-recognition receptors (PRRs). Upon detection of invasion by pathogens, PRRs activate downstream signaling pathways leading to the expression of various cytokines and immune-related genes for clearing the pathogens including bacteria, viruses, and others (Akira et al., 2006). With regards to SARS-CoV-2 infection, an overaggressive immune response that causes immunopathology has been noted (Huang et al., 2020; Zhang et al., 2020). In addition, T cell exhaustion or dysfunction has also been observed (Diao et al., 2020; Zheng et al., 2020a; Zheng et al., 2020b). Additional studies suggest that there could be a unique immune response evoked by coronaviruses (Blanco-Melo et al., 2020). However, the nature of these responses elicited by the virus remains poorly understood.

Accumulating evidence suggests that the neutrophil count is significantly increased in COVID-19 patients with severe symptoms (Kuri-Cervantes et al., 2020; Liao et al., 2020; Tan et al., 2020; Wu et al., 2020a). It is believed that in response to inflammatory stimuli neutrophils migrate from the circulating blood to infected tissues, where they protect the host by phagocytizing, killing, and digesting bacterial and fungal pathogens (Nauseef and Borregaard, 2014; Nicolás-Ávila et al., 2017). The role of such a response in host defense against viral infection has not been clearly characterized. A recent study observed a new

CellPress
OPEN ACCESS

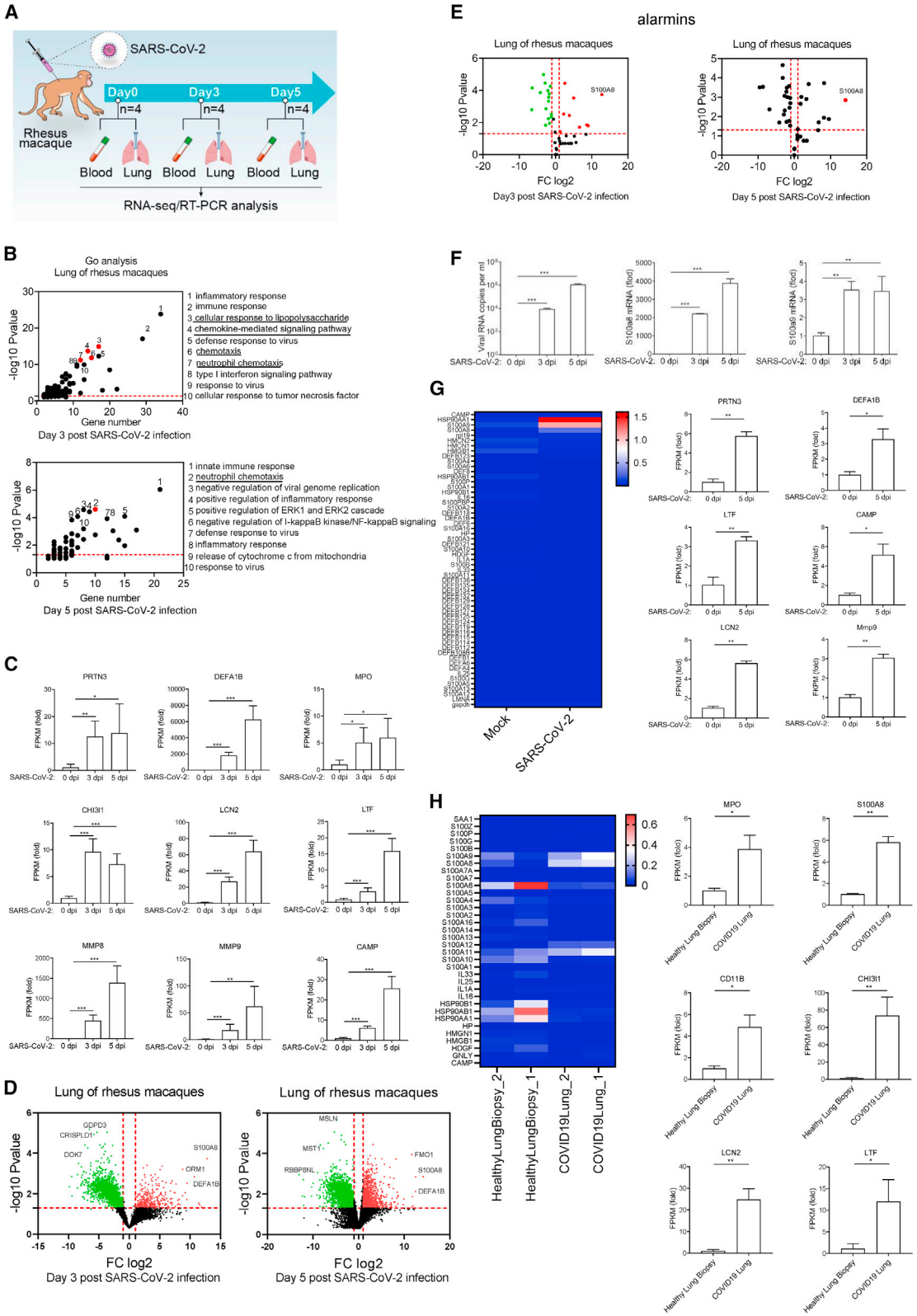

(legend on next page)

subpopulation of neutrophils in COVID-19 patients, which has been named developing neutrophils because they lack canonical neutrophil markers like CXCR2 and FCGR3B (Wilk et al., 2020). However, it is still not clear how this type of neutrophil is induced. Moreover, the precise function of these cells is also unknown.

Alarmins are endogenous, chemotactic, and immune-activating proteins/peptides that are released as a result of cell injury or death and degranulation or in response to infection. They relay intercellular defense signals by interacting with PRRs to activate immune cells in host defense (Oppenheim and Yang, 2005; Yang et al., 2017). Currently, the major categories of alarmins include defensins, high-mobility group (HMG) proteins, interleukins (ILs), heat shock proteins (HSPs), S100 proteins, uric acid, hepatoma derived growth factor (HDGF), eosinophil-derived neurotoxin (EDN), and cathelin-related anti-microbial peptide (CRAMP) (Giri et al., 2016; Yang et al., 2017). In response to microbial infection, alarmins are released to initiate and amplify innate/inflammatory immune responses, which involve the activation of resident leukocytes (e.g., macrophages, dendritic cells, mast cells, etc.), production of inflammatory mediators (cytokines, chemokines, and lipid metabolites), recruitment of neutrophils and monocytes/macrophages for the purpose of eliminating invading microorganisms, and clearing injured tissues (Bianchi, 2007; Chen and Nuñez, 2010; Nathan, 2002; Oppenheim and Yang, 2005; Yang et al., 2017). However, uncontrolled production of alarmins is harmful or even fatal to the host in some cases. HMGB1 protein acts as a late mediator of lethal systemic inflammation in sepsis (Wang et al., 2004). Therefore, anti-HMGB1 therapeutics have shown to be beneficial in experimental models of sepsis.

S100A8 and S100A9, members of the S100 group of proteins, make up approximately 45% of the cytoplasmic proteins present in neutrophils. They are also referred to as MRP8 and MRP14, respectively. Under physiological conditions, massive levels of S100A8 and S100A9 are stored in neutrophils and myeloid-derived dendritic cells, whereas low levels of S100A8 and S100A9 are expressed constitutively in monocytes (Foell et al., 2004; Wang et al., 2018). S100A8 and S100A9 often form heterodimers (S100A8/A9) (Ometto et al., 2017). The major functions of S100A8/A9 reported so far include the regulation of leukocyte migration and trafficking, the remodeling of cytoskeleton and amplification of inflammation, and exertion of anti-microbial activity (Ometto et al., 2017; Wang et al., 2018). After being infected with bacteria, neutrophils, macrophages, and monocytes intensely induce the expression and secretion of S100A8/A9 to modulate inflammatory processes through the induction of inflammatory cytokines. S100A8/A9 is an endogenous ligand of Toll-like receptor 4 (TLR4) and can trigger multiple inflammatory pathways mediated by TLR4 (Vogl et al., 2007). The receptor for advanced glycation end product (RAGE) pathways can also be activated by S100A8/A9 (Narumi et al., 2015). S100A8 and S100A9 also have anti-bacterial potential via their ability to bind Zn^{2+} (Foell et al., 2004; Wang et al., 2018). However, not much is known about the roles of S100A8/A9 in host defense responses against viruses.

In the present study, we characterized the nature of the early innate immune responses evoked in rhesus macaques and mice during SARS-CoV-2 infection. S100A8 was dramatically upregulated by SARS-CoV-2 and a mouse coronavirus (mouse hepatitis virus, MHV), but not by other viruses. A group of non-canonical aberrant neutrophils were activated during SARS-CoV-2 infection. The abnormal immune responses were mediated by the S100A8/A9-TLR4 pathway. The S100A8/A9-specific inhibitor, Paquinimod, significantly reduced the number of aberrant neutrophils induced by the coronavirus, inhibited viral replication, and rescued lung damage. These results highlight the potential of therapeutically targeting S100A8/A9 for suppressing the uncontrolled immune response associated with severe cases of COVID-19 and provide information on alarmin-mediated pathway for regulating neutrophils.

RESULTS

SARS-CoV-2 infection induces alarmin *S100A8* expression and neutrophil chemotaxis

To characterize the early immune responses against SARS-CoV-2 infection, we infected rhesus macaques with SARS-CoV-2 and analyzed the transcriptome of lung and blood at days 0, 3, and 5 post-infection (dpi) (Figures 1A and S1A). Gene ontology (GO) analysis showed that a small group of genes involved in defense responses against viruses were induced in the infected lungs (Figure 1B), and type I interferons (IFNs) were not induced by SARS-CoV-2 infection (Figure S1B). However, interestingly, a greater number of genes involved in regulating cellular responses to lipopolysaccharide (LPS) and neutrophil chemotaxis were induced (Figure 1B). Kyoto Encyclopedia of Genes and Genomes (KEGG) pathway analysis also showed that

Figure 1. *S100A8* and neutrophil-related gene expressions were significantly induced in the early stage of SARS-CoV-2 infection

(A) A flow chart depicting the process of animal experiments with rhesus macaques. Rhesus macaques (3–4 years old) were challenged with 10^6 TCID50 SARS-CoV-2 virus by intratracheal routes.

(B) Go analysis of the differences in rhesus macaques infected with SARS-CoV-2 in comparison with mock (fold change [FC] > 4 or < 0.25; p value < 0.05).

(C) Analysis of neutrophil marker genes expression. n = 4.

(D) Volcano plots show differentially expressed genes in rhesus macaques infected with SARS-CoV-2 at 3 and 5 dpi. *S100A8* expression is significantly increased after SARS-CoV-2 infection.

(E) Analysis of all known alarmins showing that *S100A8* is the most significantly induced one.

(F) qRT-PCR analysis for viral loads and the expression of *S100A8* and *S100A9* in the lungs of SARS-CoV-2-infected rhesus macaques at 3 and 5 dpi. n = 3.

(G) Heatmap shows alarmins in the blood from rhesus macaques infected with SARS-CoV-2 at 5 dpi (left). The expression of neutrophil marker genes was analyzed (FC to mock, right). n = 4.

(H) Heatmap depicting the expression of alarmins of the lung samples from healthy control and post-mortem lung samples from COVID-19 patients (left). The expression of neutrophil marker genes analyzed (FC to healthy control, right). Data from the lungs of COVID-19 patients and healthy control correspond to GEO: GSE147507.

*p < 0.05; **p < 0.01; ***p < 0.001. Error bars, SD.

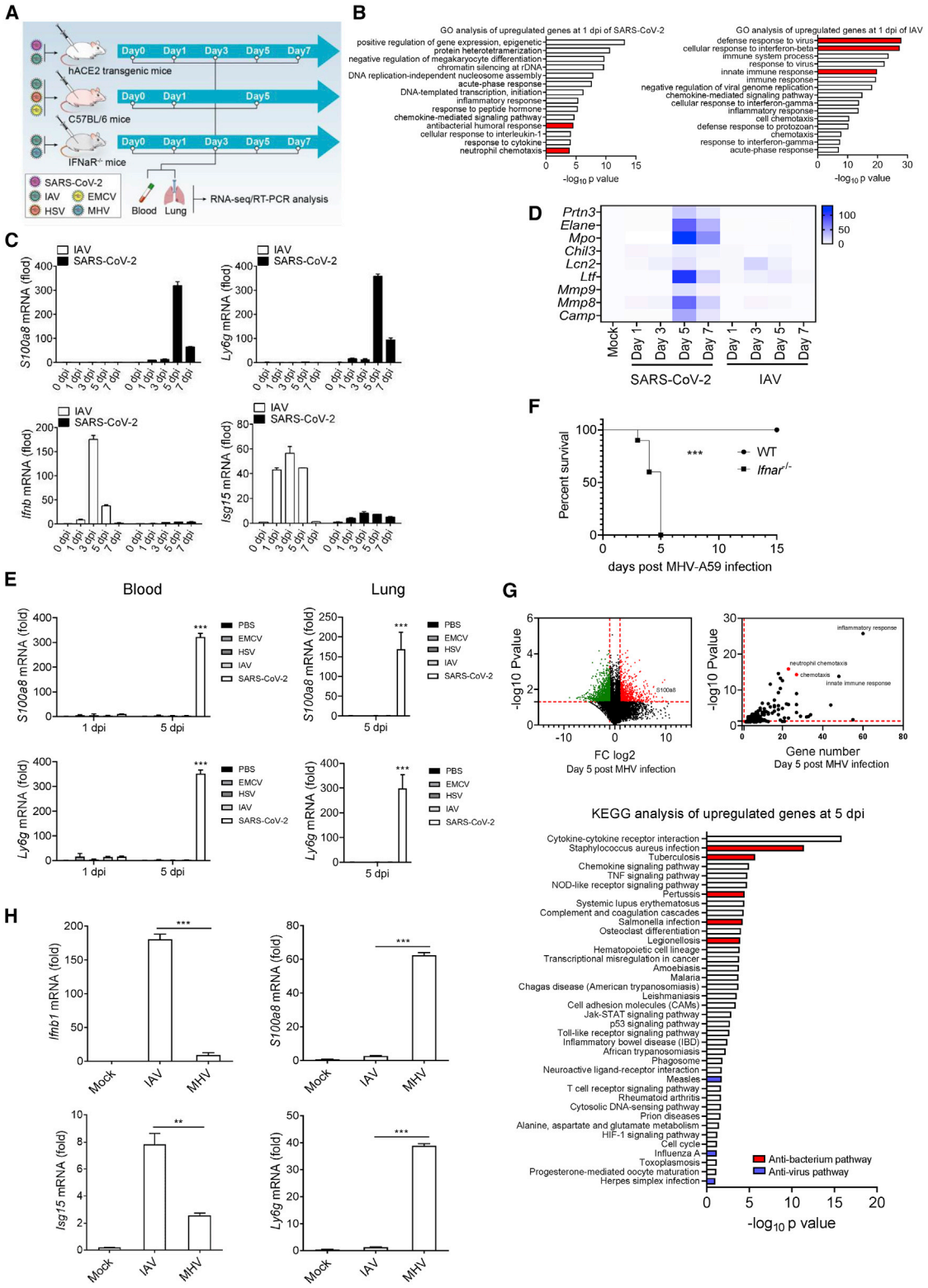

Figure 2. Anti-viral innate immune disorder and aberrant *S100a8* expression induced by coronavirus but no other viruses

(A) A flow chart depicting the process of animal experiments with mice. All the mice were inoculated intranasally with viruses. Virus doses: SARS-CoV-2 (10^5 TCID50), IAV (10^5 TCID50), EMCV (10^7 plaque-forming units [PFU]), HSV-1 (10^6 PFU), and MHV-A59 (10^5 PFU).

(B) RNA-seq analysis of lungs from mice infected with SARS-CoV-2 or IAV. Go analysis was performed with the differentially expressed genes and compared with mock (FC > 4 or < 0.25; p value < 0.05). n = 3.

(legend continued on next page)

SARS-CoV-2-induced genes were enriched in anti-bacterial pathways (Figure S1C). Meanwhile, combined with the elevated neutrophils in COVID-19 patients with severe symptoms (Kuri-Cervantes et al., 2020; Liao et al., 2020; Tan et al., 2020; Wu et al., 2020a), we hypothesized that neutrophils, which play an important anti-bacterial function, could be abnormally activated at the very beginning of SARS-CoV-2 infection. Thus, we analyzed the expression of neutrophil markers in the lungs from rhesus macaques at 0, 3, and 5 dpi. The results showed that all the neutrophil marker genes were significantly induced as a result of SARS-CoV-2 infection (Figure 1C). Markers for monocytes and natural killer cells were slightly upregulated, and T cells were unchanged, whereas B cells were significantly downregulated in the lungs of rhesus macaques infected by SARS-CoV-2 (Figures S1D and S1E). These suggested that the SARS-CoV-2 infection provoked a non-canonical anti-viral response or an anti-bacterial response accompanied by increased neutrophils in the lung at the early stage.

To explore how SARS-CoV-2 infection triggered the activation of anti-bacterial responses, the differential expression of genes before and after SARS-CoV-2 infection were examined. The results showed that the expression of *S100A8* was robustly upregulated at 3 and 5 dpi after SARS-CoV-2 infection (Figure 1D). S100A8 acts as an alarmin through formation of heterodimers with S100A9 and then functions as danger-associated molecular pattern (DAMP) molecules and activates innate immune responses via binding to PRRs, such as TLR4 (Chakraborty et al., 2017). Further, we found that S100A8 was the most significantly induced gene among all the known alarmins (Figure 1E). Subsequently, through qRT-PCR analysis, we verified that the level of *S100A8* surged along with an increase in the viral loads in the lungs of rhesus macaques infected by SARS-CoV-2 (Figure 1F). Next, we examined the expression of alarmins and neutrophil marker genes in the blood samples from infected rhesus macaques. *S100A8/A9* and the neutrophil marker genes were also induced in the blood by the SARS-CoV-2 infection (Figure 1G). We further investigated whether *S100A8* was upregulated in COVID-19 patients. Analysis of alarmins by RNA sequencing (RNA-seq) data showed that both *S100A8* and neutrophil marker genes were upregulated in post-mortem lung samples from COVID-19 patients, in comparison with biopsied healthy lung tissue from uninfected individuals (Figure 1H). Concomitantly, the mRNA level of S100A8 in peripheral blood from COVID-19-positive patients was significantly higher than in healthy subjects (Figure S1F). A group of alarmins was induced in different types of blood cells of COVID-19-positive patients, in which S100A8 was prominently induced in $CD14^+$ monocytes, neutrophils, and developing neutrophils (Figure S1G). S100A8/A9 can act as the ligand of TLR4, which is the primary PRR that recognizes invading gram-negative bacterium. Therefore, elevated *S100A8* expression could be responsible for the activation of anti-bacterial pathways and neutrophil chemotaxis. Above all, S100A8 probably play an important role in the course of SARS-CoV-2 infection.

Aberrant induction of *S100A8* is triggered by coronaviruses but not by other viruses

To further study the relationship between S100a8 expression and neutrophil chemotaxis and SARS-CoV-2 infection, we challenged human *ACE2* (*hACE2*) transgenic mice with SARS-CoV-2 and performed RNA-seq analysis of lungs to characterize the defense responses during viral infection (Figures 2A and S2A). Consistent with the results from the rhesus macaque, genes induced by SARS-CoV-2 infection in mice were also enriched in anti-bacterial humoral response and neutrophil chemotaxis and did not trigger typical anti-viral immune responses (Figures 2B and S2B). Meanwhile, *S100a8* and the neutrophil marker genes (*Ly6g, Mmp8,* etc.) were robustly upregulated at 5 dpi when the mice became sicker (Figures 2C and 2D). Consistent results across different species suggested that the sharp upregulation of *S100a8* and neutrophil chemotaxis is closely related to the formation of fatal infections by SARS-CoV-2 infection.

We then constructed a mouse model of canonical pneumonia with influenza A virus (IAV) (Figure S2C). RNA-seq analysis of lungs showed that, in comparison with SARS-CoV-2 infection, IAV infection-induced genes were enriched in defense response to virus and cellular response to IFNβ (Figures 2B and S2B). We further analyzed the differentially induced genes by SARS-CoV-2 and IAV at different time intervals after infection. The results showed that IAV induced canonical anti-viral responses and activated type I IFN signaling, whereas the expression of the classical anti-viral molecules *Ifnb1* and *Isg15* was severely impaired, and the anti-bacterial responses and neutrophil-related processes were induced during SARS-CoV-2 infection (Figures 2C, S2D, and S2E). However, IAV infection did not induce *S100a8* and neutrophil marker gene expression (Figures 2C, 2D, and S2F). These suggested that the intense expression of *S100a8* and neutrophil chemotaxis was specifically present during SARS-CoV-2 infection.

To further confirm this, we infected C57BL/6 mice with other RNA or DNA viruses including encephalomyocarditis virus (EMCV) and herpes simplex virus 1 (HSV-1) and measured the expression of S100A8 in the blood and lungs of infected animals. Neither of these viruses were able to induce the expression of *S100a8* (Figure 2E). We investigated whether other coronaviruses were able to induce the transcription of *S100a8* and neutrophil chemotaxis. We first infected C57BL/6 mice with MHV-A59 intranasally. However, no obvious symptoms in infected mice were observed. Further, we infected IRF3/IRF7 double-knockout mice and IFNAR (interferon-α

(C) qRT-PCR analysis for the expression of *S100a8*, *Ly6g*, *Ifnb*, and *Isg15* in the lungs of mice at different time points after IAV or SARS-CoV-2 infection. n = 3.
(D) Heatmap depicting the expression differences of neutrophil marker genes in the lungs of mice infected with IAV or SARS-CoV-2.
(E) qRT-PCR analysis for the expression of *S100a8* and *Ly6g* in the blood and lungs of mice infected with different viruses. n = 3.
(F) Post-infection survival curves of wild-type mice and $Ifnar^{-/-}$ mice infected with MHV. n = 10.
(G) RNA-seq analysis of the lungs of $Ifnar^{-/-}$ mice infected with MHV at 5 dpi. Go and KEGG analysis were performed with the differentially expressed genes and compared with mock (FC > 4 or < 0.25; p value < 0.05).
(H) qRT-PCR analysis for the expression of *Ifnb*, *Isg15*, *S100a8*, and *Ly6g* in the lungs of $Ifnar^{-/-}$ mice infected with IAV or MHV at 5 dpi. n = 3.
*p < 0.05; **p < 0.01; ***p < 0.001. Error bars, SD.

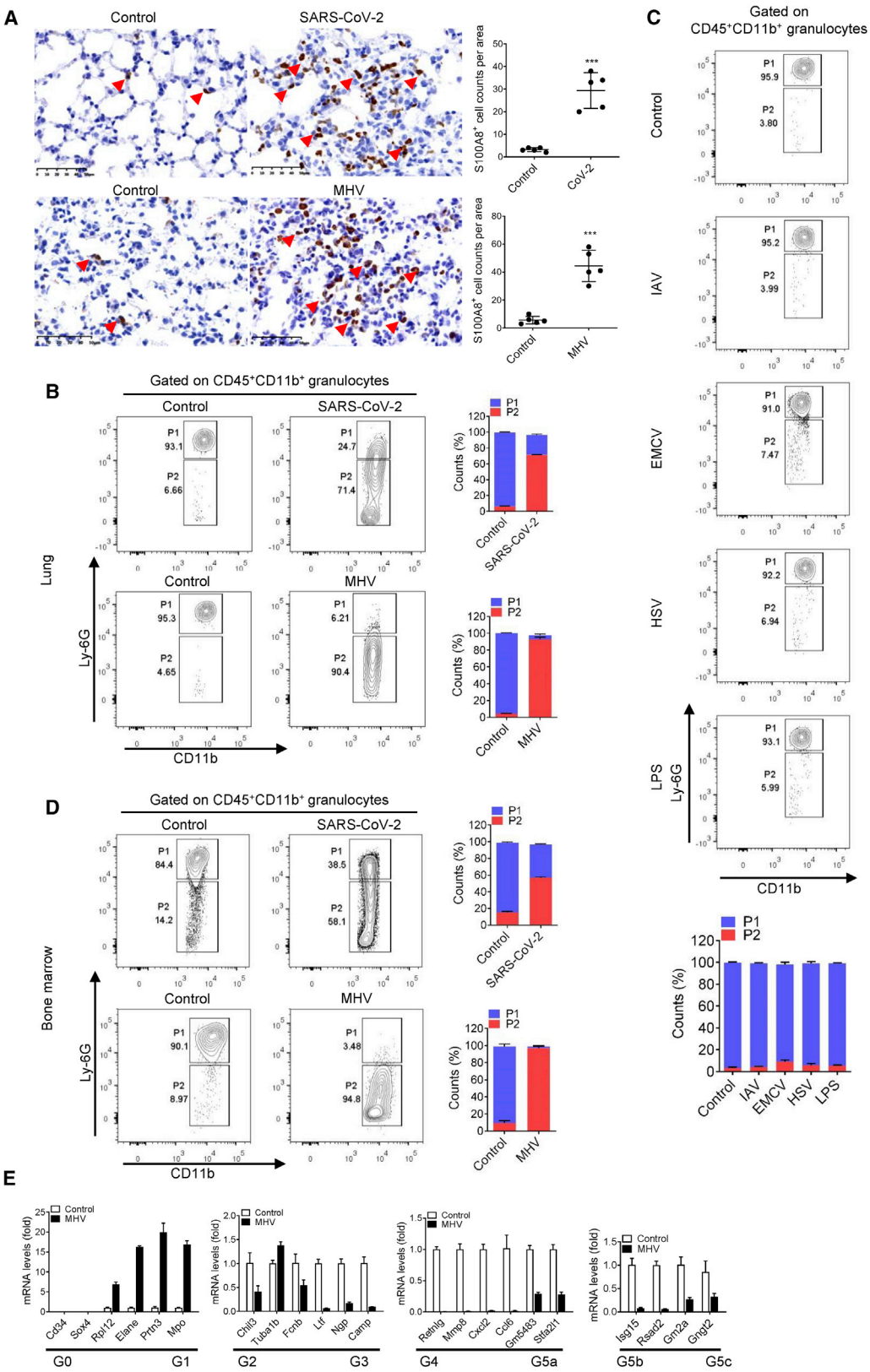

(legend on next page)

receptor)-deficient mice with MHV. Similar to the wild-type C57BL/6 mice, IRF3/IRF7 double-knockout mice were able to eliminate the virus rapidly and did not develop severe pneumonia. Interestingly, we found that all the IFNAR-deficient mice infected with MHV suddenly became sicker and died with a sharp increase in *S100a8* and *Ly6g* at 3–7 dpi, and the lungs of infected mice showed obvious lesions (Figures 2F and S3A). Meanwhile, RNA-seq analysis of the lungs showed that the genes induced by MHV were also enriched in neutrophil chemotaxis and anti-bacterial pathways (Figure 2G). In comparison with IAV infection, type I IFN induction was impaired, and neutrophil marker genes were significantly induced in MHV infection (Figures 2H, S2E, S3B, and S3C). Taken together, SARS-CoV-2 and MHV, both coronaviruses, induced an almost uniform immune response. Thus, *S100a8* expression and neutrophil chemotaxis is likely a specific feature of coronavirus infection and is involved in the formation of fatal coronavirus infections.

Coronavirus infection induces the invasion of aberrant neutrophils

The activation of anti-bacterial pathway, neutrophil chemotaxis, and high expression of *S100a8* all indicated the abnormality of neutrophils in coronavirus infection including SARS-CoV-2 and MHV. Therefore, we examined neutrophil infiltration in the lungs of infected mice. As the main cytoplasmic protein of neutrophils, S100A8 can accurately indicate neutrophils in lung tissue. Thus, immunohistochemical staining for S100A8 of the lungs in SARS-CoV-2 infection and MHV infection at 5 dpi was performed. The results showed that, in comparison with the control group, neutrophils ($S100A8^+$) invading the lungs were significantly increased in both SARS-CoV-2 and MHV infection (Figure 3A). This suggested that coronavirus infection does induce the invasion of neutrophils.

To further accurately define neutrophil invasion during SARS-CoV-2 and MHV infection, the neutrophils in the lungs of infected mice were analyzed by flow cytometry (Figure S4A). The results showed that almost all the neutrophils in the control group were typical $CD45^+CD11b^+Ly6G^{high}$. Surprisingly, however, most neutrophils in SARS-CoV-2- and MHV-infected mice showed $CD45^+CD11b^+Ly6G^{variable}$ (Figure 3B). This indicated that neutrophils in coronavirus-infected mice were distorted. To investigate whether other viruses or stimuli are able to induce the production of this particular group of neutrophils, we challenged mice with IAV, EMCV, HSV, and LPS. The results showed that although these infections caused fluctuations in the number of neutrophils, these neutrophils were still $CD45^+CD11b^+Ly6G^{high}$ and did not appear abnormal (Figure 3C). These suggested that coronavirus infection induced the invasion of a group of aberrant neutrophils.

To investigate the source of this population of aberrant neutrophils, we analyzed the peripheral blood and bone marrow of coronavirus-infected mice by flow cytometry. Shockingly, neutrophils were also aberrant in the peripheral blood of SARS-CoV-2- and MHV-infected mice, even in the bone marrow (Figures 3D and S4B). The relatively low Ly-6G levels in aberrant neutrophils suggested that it could be an immature cell. Further, we purified the aberrant neutrophils in bone marrow of MHV-infected mice by flow cytometry sorting and analyzed the expression of marker gene (*Cxcr2* and *Fcgr3*) of mature neutrophils in these aberrant neutrophils. The qRT-PCR results showed that, in comparison with the expression of *Cxcr2* and *Fcgr3* in normal neutrophils in control group, the expression of *Cxcr2* and *Fcgr3* in these aberrant neutrophils were significantly reduced, which indicated their immature characteristics (Figure S4C). A recent single-cell sequencing data clarified the heterogeneity of neutrophil development and identified eight (G0-G5c) developing neutrophil subpopulations by 24 marker genes (Xie et al., 2020). From this, the expression of the 24 marker genes in aberrant neutrophils was also analyzed. The results showed that, in comparison with the normal neutrophils in control group, only the expression of G1 maker genes were significantly increased in these aberrant neutrophils (Figure 3E). This suggested that these abnormal neutrophils were similar to the G1 developing neutrophils. In addition, the RNA-seq data of lungs in mice infected by SARS-CoV-2 and IAV also showed that the G5b mature neutrophils were primarily activated in IAV infection, whereas most neutrophils recruited in SARS-CoV-2 infection are at stages of G1 to G4 subpopulation (Figures S4D and S4E). Together, these suggested that coronavirus infection induced a population of dysplastic aberrant neutrophils and could cause the dysregulation of the innate immune system.

Paquinimod suppresses the accumulation of aberrant neutrophils and coronavirus infection

Aberrant neutrophils coiled around the emergence of symptoms in mice, suggesting that they could be responsible for the fatal infection of coronavirus. Additionally, as the main cytoplasmic protein of neutrophils, S100A8 has great influence on the function of neutrophils. Therefore, to further clarify the role of S100A8 in the emergence of the aberrant neutrophils and coronavirus infection, we designed experiments to suppress the effects of S100A8/A9. Paquinimod can prevent the binding of S100A9 to TLR4 (Björk et al., 2009; Schelbergen et al., 2015), suggesting that it can be used to block the function of

Figure 3. A group of immature aberrant neutrophils emerged in coronavirus-infected mice

(A) Immunohistochemical analysis of the location and expression of S100A8 in the lung tissue of mice infected with SARS-CoV-2 or MHV at 5 dpi. The $S100A8^+$ cells in the lungs of mice infected with coronavirus were increased significantly. The red arrows indicate the $S100A8^+$ cells. n = 5. Scale bars, 50 μm.

(B) Flow cytometry analysis of neutrophils in lungs from mice infected with SARS-CoV-2 and MHV at 5 dpi. Control group means mice treated with vehicle. Gate P1 shows the conventional neutrophils ($CD45^+CD11b^+Ly6G^{high}$), and Gate P2 shows the pathologic aberrant neutrophils ($CD45^+CD11b^+Ly6G^{variable}$). Aberrant neutrophils (P2) in the lungs of mice infected with coronavirus were significantly increased. n = 3.

(C) Flow cytometry analysis of neutrophils in lungs of mice challenged with IAV, EMCV, HSV-1, and LPS at 5 dpi. The results showed that these treatments did not induce an increase in aberrant neutrophils. n = 3.

(D) Flow cytometry analysis of neutrophils in bone marrow from mice infected with SARS-CoV-2 and MHV at 5 dpi. n = 3.

(E) qRT-PCR-analyzed related gene expression of aberrant neutrophils in bone marrow of mice infected with MHV at 5 dpi and identified the differentiated types of aberrant neutrophils. n = 3.

***$p < 0.001$. Error bars, SD.

CellPress
OPEN ACCESS

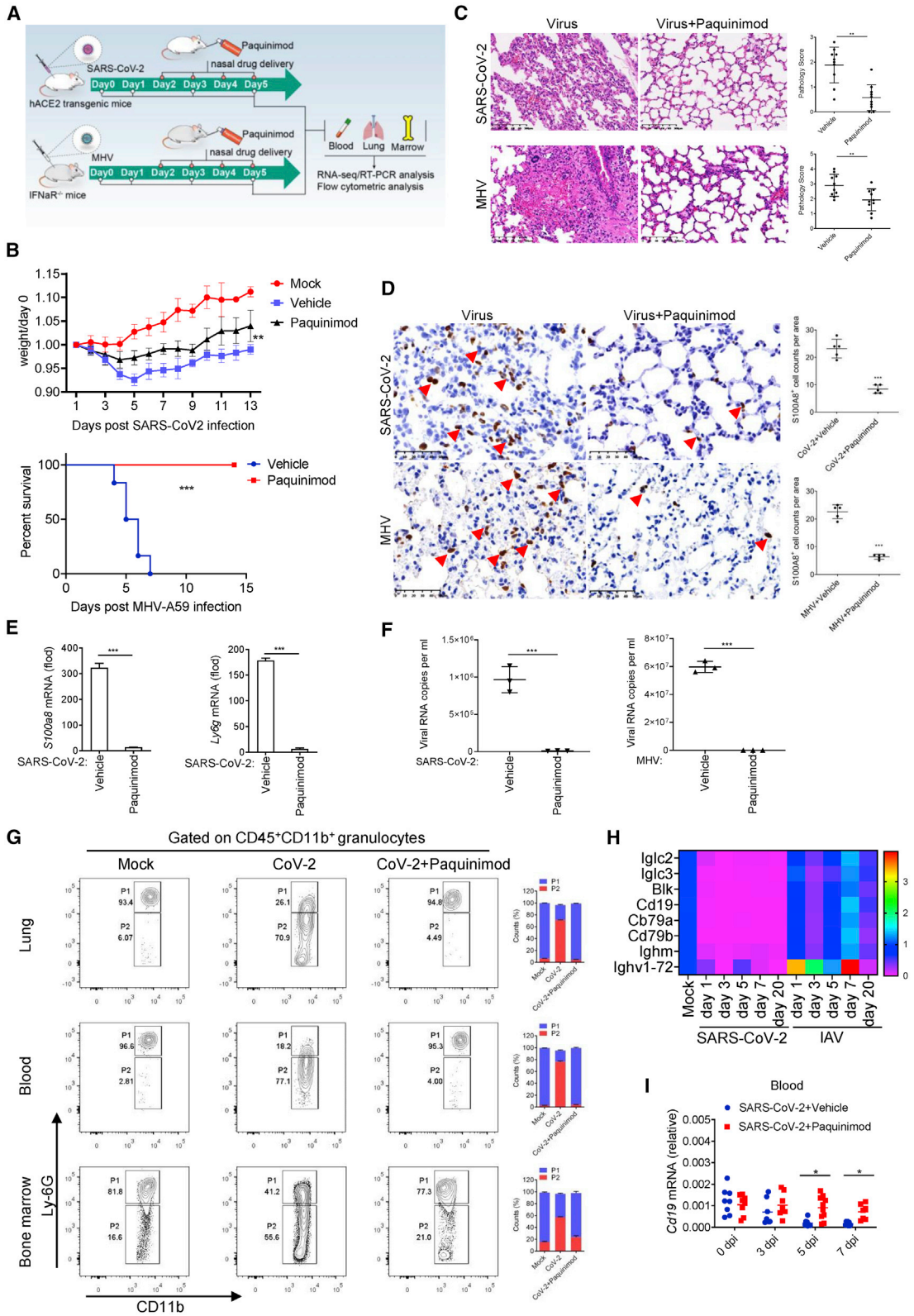

Figure 4. Paquinimod rescues the mice infected by SARS-CoV-2 and MHV

(A) A flow chart depicting the process of a drug rescue experiment.

(B) Analysis of weight and survival rate of mice infected with SARS-CoV-2 and MHV after Paquinimod treatment. n = 6.

(legend continued on next page)

S100A8/A9. Thus, we treated the mice intranasally with Paquinimod after SARS-CoV-2 and MHV infection (Figure 4A). Excitingly, the treatment of Paquinimod successfully improved the living state of mice (Figure 4B). Histopathological and immunohistochemical staining of the lungs showed that both the pulmonary interstitium damage and the invasion of neutrophils (S100A8$^+$) were alleviated via Paquinimod treatment (Figures 4C and 4D). Further detection found that *S100a8* and *Ly6g* expression and viral loads including SARS-CoV-2 and MHV in the mice that were successfully rescued by Paquinimod were significantly reduced (Figures 4E, 4F, S5A, and S5B). Subsequently, neutrophils in Paquinimod-treated mice were analyzed by flow cytometry. As expected, in comparison with the coronavirus infection group, most neutrophils in Paquinimod-treated mice returned to normal CD45$^+$CD11b$^+$Ly6G^{high} levels (Figures 4G and S5C). These results indicated that Paquinimod successfully rescued mice from fatal outcome from coronavirus infection. However, Paquinimod did not succeed in rescuing IAV-infected mice that did not show high *S100a8* expression and aberrant neutrophils (Figures 2C and S5D). Paquinimod likely blocked the function of S100A8/A9 specifically, thereby preventing the accumulation of aberrant neutrophils and fatal coronavirus infection.

To evaluate the effect of Paquinimod on the modulation of immune responses in coronavirus-infected mice, the RNA-seq analysis of lungs was performed. In the case of MHV infection, neutrophil chemotaxis and anti-bacterial responses were significantly downregulated after Paquinimod treatment (Figure S5E). The expression of neutrophil marker genes was also reduced by Paquinimod (Figure S5F). Meanwhile, as an important component of the adaptive immune system that plays a major anti-viral role, B cell signaling pathways are significantly activated after Paquinimod treatment (Figures 4E and S5G). Further qRT-PCR analysis showed that, consistent with MHV infection, the B cell marker gene *Cd19* in SARS-CoV-2 infection was also gradually restored and showed a tendency of upregulation after Paquinimod treatment (Figures 4H, 4I, and S5H). These suggested that Paquinimod treatment contributed to the recovery of the aberrant immune response caused by the coronavirus, which in turn promotes the elimination of the virus.

S100A8/A9 mediates the emergence of aberrant neutrophils in a TLR4-dependent manner

Paquinimod treatment, which is able to inhibit the function of S100A8/A9 by blocking the binding of S100A9 to TLR4, suppressed the accumulation of aberrant neutrophils and rescued mice from fatal coronavirus infection. This suggested that the TLR4 signaling pathway could play an important role in coronavirus-induced fatal infections. To make this clear, we treated mice infected by coronavirus including SARS-CoV-2 and MHV with TLR4 signaling inhibitor. Resatorvid is a selective TLR4 inhibitor that can downregulate expression of TLR4 downstream signaling molecules. Through Resatorvid treatment, we found that the proportion of aberrant neutrophils in coronavirus-infected mice were significantly reduced (Figures 5A and 5B). Consistently, Resatorvid also inhibited *S100a8* and *Ly6g* expression and viral replication in lungs of the infected mice (Figures 5C and 5D). Besides, it is believed that S100A8/A9 can also activate the RAGE pathways (Narumi et al., 2015). To this end, we also treated mice infected by SARS-CoV-2 and MHV with RAGE inhibitor (Azeliragon). The results showed that Azeliragon treatment did not significantly prevent the production of aberrant neutrophils and viral replication (Figures S6A and S6B). This implied the critical role of the TLR4 signaling pathway in coronavirus infection. A previous study showed that S100A8/A9 can promote granulopoiesis by activating macrophages and common myeloid progenitor (Nagareddy et al., 2013). Thus, to further confirm the role of TLR4 in activating S100A8-related signaling, we treated wild-type or MyD88-deficient mouse macrophages Raw264.7 with the recombinant S100A8/A9. MyD88 is an important adaptor protein, and the absence of MyD88 can lead to the suppression of TLR4 signaling (Figure S6C). The detection results showed that recombinant S100A8/A9 was able to induce the expression of *S100a8* and neutrophil chemokine *Cxcl2* in a TLR4-/MyD88-dependent manner (Figure 5E). This reflected that S100A8 was able to induce the expression of itself, thereby forming a positive loop and amplifying the aberrant responses.

DISCUSSION

The endogenous DAMPs are able to trigger the activation of innate immune signaling. Alarmins are a panel of proteins or peptides that can function as DAMPs to activate various immune pathways (Bianchi, 2007; Yang et al., 2017). The fine tuning of alarmin expression is critical for maintaining immune homeostasis. Over- or sustained expression of alarmins can result in uncontrolled inflammation and cytokine storm (Chan et al., 2012; Cher et al., 2018; Kang et al., 2014; Patel, 2018). Here, we demonstrated that coronavirus, such as SARS-CoV-2 and MHV, induced a robust transcription of the alarmin S100A8, which in turn led to innate anti-viral immune disorder. These results were consistent with the recent studies that revealed that

(C) Analysis of the rescue effect of Paquinimod by H&E staining and pathology score of lung tissue in mice infected with SARS-CoV-2 or MHV at 5 dpi. Paquinimod treatment significantly prevented the bleeding and fibrosis in lung tissue. A number of pulmonary H&E staining images were randomly selected for pathological scoring. n = 10. Scale bars, 100 μm.
(D) Immunohistochemical analysis of the S100A8$^+$ cells in the lung tissue of mice infected with SARS-CoV-2 or MHV at 5 dpi after Paquinimod treatment. The S100A8$^+$ cells in the lungs of mice infected with coronavirus were decreased significantly after Paquinimod treatment. The red arrows indicate the S100A8$^+$ cells. n = 5. Scale bars, 50 μm.
(E) qRT-PCR analysis for the expression of *S100a8* and *Ly6g* in the lung of mice infected with SARS-CoV-2 at 5 dpi after Paquinimod treatment. n = 3.
(F) qRT-PCR analysis of viral loads in the lungs of mice infected with coronavirus SARS-CoV-2 and MHV at 5 dpi after Paquinimod treatment. n = 3.
(G) Flow cytometry analysis of neutrophils in lungs, blood, and bone marrow from mice infected with SARS-CoV-2 at 5 dpi after Paquinimod treatment. CD45$^+$CD11b$^+$Ly6G^{variable} aberrant neutrophils (P2) in the mice infected with SARS-CoV-2 were significantly decreased by Paquinimod treatment. n = 3.
(H) Heatmap depicting a decrease in B cell-related gene expression in the lungs of mice infected with SARS-CoV-2.
(I) qRT-PCR analysis for the expression of B cell marker gene *Cd19* in the peripheral blood of mice infected with SARS-CoV-2 after Paquinimod treatment. n ≥ 5.
*p < 0.05; **p < 0.01; ***p < 0.001. Error bars, SD.

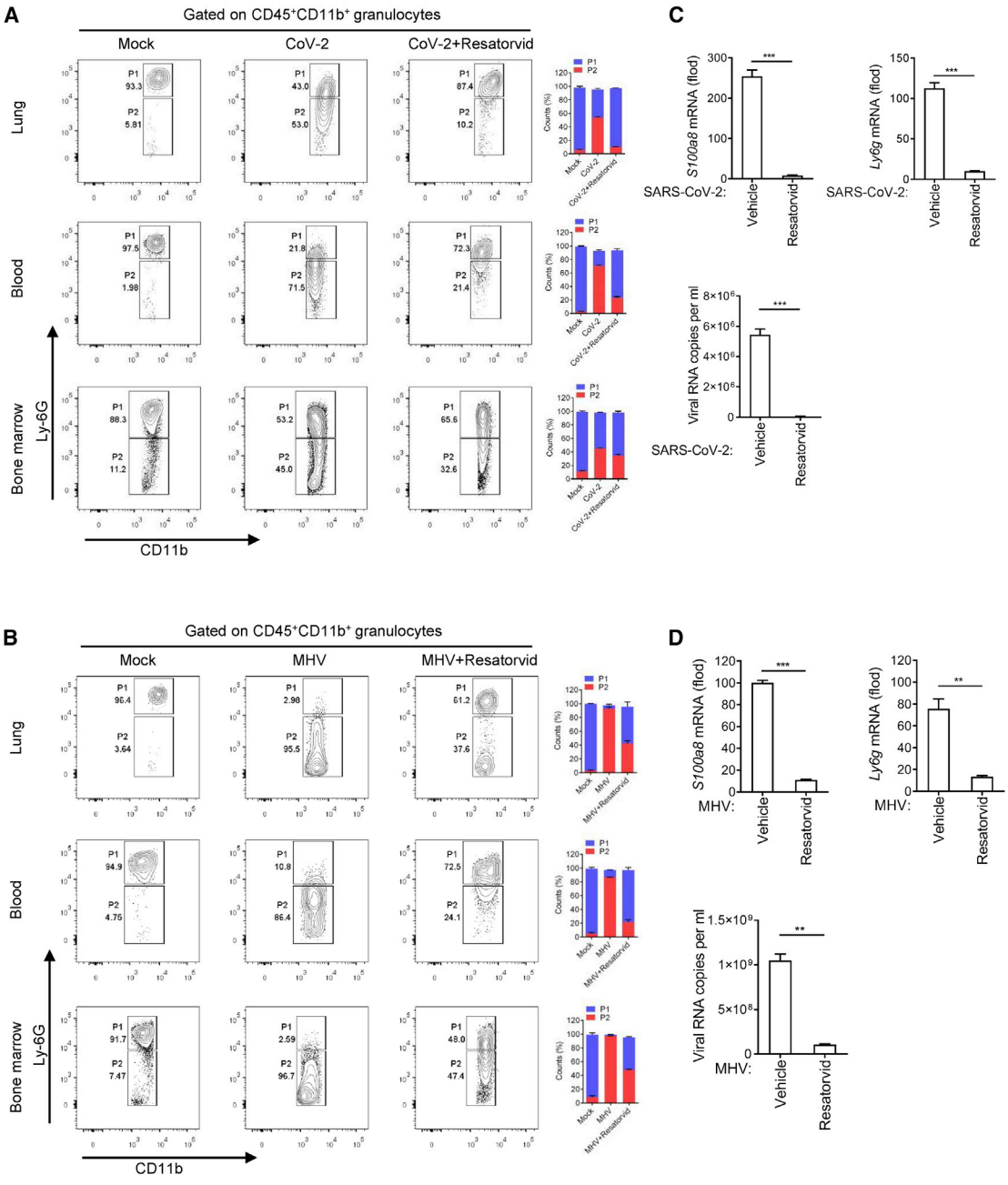

(legend on next page)

S100A8/A9 (calprotectin) was highly elevated in patients with COVID-19 and was a prognosticator of negative outcomes (Shi et al., 2020; Silvin et al., 2020). In addition to S100A8, several alarmins had also been found to be upregulated in COVID-19 patients, which could be influenced by multiple factors, such as the course of the disease, treatment drugs, and so on. Therefore, their role in COVID-19 patients still needs to be further explored. During SARS-CoV-2 infection, the induction of type I IFNs is inhibited and neutrophils respond abnormally, and similar phenotypes were observed during MHV infection. The type I IFNs are the primary anti-viral effectors that are usually induced at the very early stage of viral infection. Thus, the inhibition of type I IFNs suggests a disruption of the classical anti-viral immune response. Meanwhile, a good deal of literature has shown that the induction of type I IFNs was also suppressed during SARS-CoV infection (Channappanavar et al., 2016; Chu et al., 2020; Frieman et al., 2010; Matsuyama et al., 2020; Zornetzer et al., 2010). These studies suggested that delayed type I IFN induction was responsible for lethal pneumonia in SARS-COV-infected mice. Therefore, exploring the mechanism of type I IFN suppression could be of great significance for the containment of coronavirus infection.

IFNAR-deficient mice have been suggested as a potential animal model for SARS-CoV-2 experiments (Hanifehnezhad et al., 2020). In this study, we attempted to establish a mouse model of coronavirus-related severe acute respiratory distress syndrome (ARDS) by MHV. The results showed that in IFNAR-deficient mice, MHV successfully invaded the lung of the mice and induced an immune response similar to SARS-CoV-2 infection. This suggested that it seems like a shared mechanism that directs the pathogenesis of pneumonia during SARS-CoV-2 infection and MHV infection. Thus, IFNAR-deficient mice infected by MHV could serve as useful models for investigating ARDS associated with SARS-CoV-2 infection. Besides, the susceptibility of IFNAR-deficient mice to coronavirus suggested that the type I IFN signaling pathway could be important for resistance to coronavirus infection. IRF3 and IRF7 are key transcription factors of type I IFNs (You et al., 2013). However, IRF3/IRF7 double-knockout mice challenged with MHV did not develop obvious ARDS. Additionally, previous studies and as well as our own data showed that induction of type I IFNs is blocked during SARS-CoV-2 and MHV infection (Hadjadj et al., 2020; Zhou et al., 2020). These suggested that IFNAR could exert an unknown mechanism during resistance to coronavirus infection in a way independent of type I IFNs.

Neutrophil abnormalities were defined during SARS-CoV-2 infection through our study. Neutrophils are usually activated during bacterial infection to kill invading bacteria (Deng et al., 2013; Li et al., 2002). However, in COVID-19 patients with severe symptoms, neutrophils were found to be significantly increased (Kuri-Cervantes et al., 2020; Liao et al., 2020; Tan et al., 2020; Wu et al., 2020a). It was originally thought that the increase in neutrophils in severe COVID-19 patients could be attributed to co-infection of bacteria. However, several reports, including our study, have found that the increase of neutrophils was not due to bacterial co-infection but to a group of aberrant neutrophils induced by SARS-CoV-2 infection. Further, both our study and recent studies have identified that these abnormal neutrophils showed obvious immature characteristics (Schulte-Schrepping et al., 2020; Silvin et al., 2020; Wilk et al., 2020). This is consistent with the basic characteristics of myeloid-derived suppressor cells (MDSCs). The presence of G-MDSCs could explain reduced white-blood-cell levels in severe COVID-19 patients. Besides, the current study also found that thrombosis in COVID-19 was associated with higher levels of circulating neutrophil extracellular traps (NETs) and calprotectin (S100A8/A9) (Shi et al., 2020; Zuo et al., 2020). The formation of NETs is one of the main ways in which neutrophils function (Ali et al., 2019; Meng et al., 2017; Yadav et al., 2019). Therefore, it is worthwhile to investigate whether these aberrant neutrophils cause the increase and dysfunction of circulating NETs. In short, the exact function of these aberrant neutrophils and the mechanism of aberrant neutrophils induced by coronavirus infection remain to be further explored.

Our study showed the importance of the TLR4 signaling pathway in the formation of fatal infections by coronavirus. Through blocking TLR4 signaling, both Paquinimod and Resatorvid improved the health status of coronavirus-infected mice. Previous SARS-CoV studies also showed that TLRs, including TLR3, TLR4, TLR7, and TLR8, mediated anti-viral responses (Li et al., 2016; Li et al., 2013; Totura et al., 2015). Meanwhile, *Tlr3*$^{-/-}$ and *Tlr4*$^{-/-}$ mice also showed greater susceptibility to SARS-CoV than did wild-type mice, and the deficiency of TLR adaptor proteins TRIF or MyD88 resulted in higher mortality of mice during SARS-CoV infection (Totura et al., 2015). All these suggested that TLR signaling also plays an important role in SARS-CoV infection, which further reflects the close relationship between TLR signals and coronavirus infection. However, it was previously unknown how TLR4 signaling was activated by coronavirus infection. Here, we found that the sharp upregulation of S100A8 in coronavirus infection could be responsible for activation of TLR4 signaling. S100A8 is the main cytoplasmic protein of mature neutrophils. Thus, during the initial phase of SARS-CoV-2 infection, *S100a8* was slightly induced in lungs at 1dpi, possibly due to the recruitment of mature neutrophils into the lungs (Figure 2C). The RNA-seq data also showed that the marker gene *Cxcr2* of mature neutrophils was upregulated at 1 dpi during SARS-CoV-2 infection. Thus, it is possible that mature neutrophils that invaded the lungs carried large amounts of S100A8/A9, which can further induce the expression of itself. This could form a positive loop to amplify the aberrant response. Excessive and uncontrolled S100A8/A9 production strongly stimulates the

Figure 5. Blocking TLR4 signal can alleviate coronavirus fatal infection

(A and B) Flow cytometry analysis of neutrophils in lungs, blood, and bone marrow from mice infected with SARS-CoV-2 (A) and MHV (B) at 5 dpi after Resatorvid treatment. Aberrant neutrophils (P2) in the mice infected with coronavirus were significantly decreased by Resatorvid treatment. n = 3.

(C and D) qRT-PCR analysis for the expression of *S100a8*, *Ly6g*, and viral loads in the lungs of mice infected with SARS-CoV-2 (C) and MHV (D) at 5 dpi after Resatorvid treatment. n = 3.

(E) qRT-PCR analysis for the effect of recombinant S100A8/A9 on *S100a8* and *Cxcl2* expression through TLR4 pathway. n = 3.

*p < 0.05; **p < 0.01; ***p < 0.001. Error bars, SD.

TLR4 signal, which induces the aberrant neutrophils and imbalance of immune response. However, the exact mechanism of S100A8 surge and TLR4 signal activation induced by coronavirus infection remains to be further explored. A recent study predicted that antigenic epitopes within the full-length S protein of SARS-CoV-2 could bind to TLR4/MD-2 complex and activate immune response (Bhattacharya et al., 2020). Based on this, there might be a possibility that SARS-CoV-2 could directly stimulate the expression of S100A8/A9 by TLR4 signaling. Because SARS-CoV-2 is an RNA virus, it is also reasonable that SARS-CoV-2 could induce neutrophilic S100A8/A9 expression by activating RNA sensing pathways, such as RIG-I (retinoic acid-inducible gene I)-like receptor, TLR3 and TLR7/8 signaling. Moreover, TLR4 of macrophages can also be activated by S100A8/A9. Although the expression level of S100A8 is low, the function of it in Raw 274.7 cells has been validated previously (Müller et al., 2017). We here also observed the induction of *S100a8* and *Cxcl2* by the treatment of S100A8/A9 (Figure 5E). Besides, the induction of proinflammatory cytokines, such as IL-1B and IL-6, in macrophages or the bronchoalveolar lavage fluid (BALF) by S100A8/A9 is also noteworthy. However, these views still need to be supported by more data in the future.

In summary, we have demonstrated that coronavirus infection including SARS-CoV-2 and MHV leads to the disorder of anti-viral innate immunity. It has been shown that alarmin S100A8 was robustly upregulated, and a group of aberrant premature neutrophils were induced. TLR4 signaling could mediate this abnormal immune response. The inhibitors of the S100A8/A9-TLR4 axis were able to mitigate the abnormality of anti-viral immunity and inhibit viral replication. These results uncover the characteristic of innate immunity in the pathogenesis of SARS-CoV-2 infection and provide therapeutic targets for the treatment of COVID-19.

Limitations of the study

In the rhesus macaque infection model, neutrophil abnormalities were only indirectly reflected by RNA-seq data and were not visualized by cell staining due to the limitations of the associated antibodies. Although we have shown that Paquinimod and Resatorvid are effective in preventing SARS-CoV-2 infection, their efficacy in rescuing rhesus macaques infected with SARS-CoV-2 was not further tested due to limited experimental conditions. The absence of severe disease in SARS-CoV-2-infected hACE2 mice largely limited the progress of the study, which could be due to the limited replication of the virus in hACE2 mice. This also makes the data on weight loss of mice seem unconvincing. Although we supplemented experimental data on mouse coronavirus MHV infection similar to SARS-CoV-2 infection, the consistency of the two coronavirus infection mechanisms cannot be fully assured. The presence of abnormal immature neutrophils could be an important cause of severe disease during SARS-CoV-2 infection. In experiments, we found that these abnormal immature neutrophils were likely MDSCs, which effectively inhibited the production and activation of other immune cells and led to immune system disorders. This could be the root cause of the virus replication outbreak, and the detailed process needs to be further explored. SARS-CoV-2 infection was effectively inhibited by targeting S100A8/A9-TLR4 axis inhibition. However, it is still unknown how SARS-CoV-2 infection induces the elevated expression of S100A8/A9 in the first place. Furthermore, the drug regimens of Paquinimod and Resatorvid need to be further optimized. In experiments, we found that poor drug use regimens had the opposite effect for reasons that are still unknown. We have developed a relatively effective drug regimen in mice, but the optimal drug regimen needs to be further explored. Collectively, the study contains many limitations, but the innate immune abnormalities and possible drug targets proposed in this study provide new therapy ideas for COVID-19.

STAR★METHODS

Detailed methods are provided in the online version of this paper and include the following:

- KEY RESOURCES TABLE
- RESOURCE AVAILABILITY
  - Lead contact
  - Materials availability
  - Data and code availability
- EXPERIMENTAL MODEL AND SUBJECT DETAILS
  - Cells
  - Viruses
  - Animal experiments
- METHOD DETAILS
  - Animal infection assays
  - RNA sequencing (RNA-seq)
  - Quantitative RT-PCR (qRT-PCR) analysis
  - Histology and immunohistochemical staining
  - Tissue preparation and flow cytometry
  - Drug rescue assay
  - Cell co-culture assay
- QUANTIFICATION AND STATISTICAL ANALYSIS
  - RNA-seq analysis
  - Data analysis for flow cytometry data
  - Statistical analysis

SUPPLEMENTAL INFORMATION

Supplemental Information can be found online at https://doi.org/10.1016/j.chom.2020.12.016.

ACKNOWLEDGMENTS

This work was supported by the National Natural Science Foundation of China (31570891; 31872736; 32022028), the National Key Research and Development Program of China (2016YFA0500302; 2020YFA0707800), the National Key Research and Development Program (2020YFA0707500) and the Strategic Priority Research Program (XDB29010000), and Peking University Clinical + X (PKU2020LCXQ009). Xiangxi Wang was supported by Ten Thousand Talent Program and the NSFS Innovative Research Group (81921005). We also thank National Mega projects of China for Major Infectious Diseases (2017ZX10304402), CAMS initiative for Innovative Medicine of China (2016-12M-2-006), and the National Natural Science Foundation of China (82041008 and 32070543) for the support on the animal model development and experiments.

AUTHOR CONTRIBUTIONS

F.Y., Xiangxi Wang, C.Q., and Q.G. conceived the study and analyzed the data. Q.G., Y.Z., J. Li, J. Liu, and Y.X. performed most experiments and analyzed the data. F.Y. and X.G. analyzed the RNA-seq data. M.K. and N.W. helped with the *in vitro* cell experiments. H.X. helped with the flow cytometry experiments.

L.B., D.W., H.Z., and R.G. helped with the rhesus macaques and *hACE2* mice-related experiments. Z.Z., L. Cao, and Y.L. helped with the other mice experiments. Y.L., Xiao Wang, X. Wei, L. Chen, and J.C. provided support on literature search. F.Y. wrote the paper. F.Y., Xiangxi Wang, and C.Q. revised the paper.

DECLARATION OF INTERESTS

The authors have no conflicts of interest to declare.

Received: August 29, 2020
Revised: November 11, 2020
Accepted: December 21, 2020
Published: December 26, 2020

REFERENCES

Akira, S., Uematsu, S., and Takeuchi, O. (2006). Pathogen recognition and innate immunity. Cell *124*, 783–801.

Ali, R.A., Gandhi, A.A., Meng, H., Yalavarthi, S., Vreede, A.P., Estes, S.K., Palmer, O.R., Bockenstedt, P.L., Pinsky, D.J., Greve, J.M., et al. (2019). Adenosine receptor agonism protects against NETosis and thrombosis in antiphospholipid syndrome. Nat. Commun. *10*, 1916.

Bao, L., Deng, W., Huang, B., Gao, H., Liu, J., Ren, L., Wei, Q., Yu, P., Xu, Y., Qi, F., et al. (2020). The pathogenicity of SARS-CoV-2 in hACE2 transgenic mice. Nature *583*, 830–833.

Bhattacharya, M., Sharma, A.R., Mallick, B., Sharma, G., Lee, S.S., and Chakraborty, C. (2020). Immunoinformatics approach to understand molecular interaction between multi-epitopic regions of SARS-CoV-2 spike-protein with TLR4/MD-2 complex. Infect. Genet. Evol. *85*, 104587.

Bianchi, M.E. (2007). DAMPs, PAMPs and alarmins: all we need to know about danger. J. Leukoc. Biol. *81*, 1–5.

Björk, P., Björk, A., Vogl, T., Stenström, M., Liberg, D., Olsson, A., Roth, J., Ivars, F., and Leanderson, T. (2009). Identification of human S100A9 as a novel target for treatment of autoimmune disease via binding to quinoline-3-carboxamides. PLoS Biol. *7*, e97.

Blanco-Melo, D., Nilsson-Payant, B.E., Liu, W.C., Uhl, S., Hoagland, D., Møller, R., Jordan, T.X., Oishi, K., Panis, M., Sachs, D., et al. (2020). Imbalanced Host Response to SARS-CoV-2 Drives Development of COVID-19. Cell *181*, 1036–1045.e9, e1039.

Chakraborty, D., Zenker, S., Rossaint, J., Hölscher, A., Pohlen, M., Zarbock, A., Roth, J., and Vogl, T. (2017). Alarmin S100A8 Activates Alveolar Epithelial Cells in the Context of Acute Lung Injury in a TLR4-Dependent Manner. Front. Immunol. *8*, 1493.

Chan, J.K., Roth, J., Oppenheim, J.J., Tracey, K.J., Vogl, T., Feldmann, M., Horwood, N., and Nanchahal, J. (2012). Alarmins: awaiting a clinical response. J. Clin. Invest. *122*, 2711–2719.

Channappanavar, R., Fehr, A.R., Vijay, R., Mack, M., Zhao, J., Meyerholz, D.K., and Perlman, S. (2016). Dysregulated Type I Interferon and Inflammatory Monocyte-Macrophage Responses Cause Lethal Pneumonia in SARS-CoV-Infected Mice. Cell Host Microbe *19*, 181–193.

Chen, G.Y., and Nuñez, G. (2010). Sterile inflammation: sensing and reacting to damage. Nat. Rev. Immunol. *10*, 826–837.

Cher, J.Z.B., Akbar, M., Kitson, S., Crowe, L.A.N., Garcia-Melchor, E., Hannah, S.C., McLean, M., Fazzi, U.G., Kerr, S.C., Murrell, G.A.C., and Millar, N.L. (2018). Alarmins in Frozen Shoulder: A Molecular Association Between Inflammation and Pain. Am. J. Sports Med. *46*, 671–678.

Chu, H., Chan, J.F., Wang, Y., Yuen, T.T., Chai, Y., Hou, Y., Shuai, H., Yang, D., Hu, B., Huang, X., et al. (2020). Comparative Replication and Immune Activation Profiles of SARS-CoV-2 and SARS-CoV in Human Lungs: An Ex Vivo Study With Implications for the Pathogenesis of COVID-19. Clin. Infect. Dis. *71*, 1400–1409.

Deng, Q., Sarris, M., Bennin, D.A., Green, J.M., Herbomel, P., and Huttenlocher, A. (2013). Localized bacterial infection induces systemic activation of neutrophils through Cxcr2 signaling in zebrafish. J. Leukoc. Biol. *93*, 761–769.

Diao, B., Wang, C., Tan, Y., Chen, X., Liu, Y., Ning, L., Chen, L., Li, M., Liu, Y., Wang, G., et al. (2020). Reduction and Functional Exhaustion of T Cells in Patients With Coronavirus Disease 2019 (COVID-19). Front. Immunol. *11*, 827.

Feng, J., Meyer, C.A., Wang, Q., Liu, J.S., Shirley Liu, X., and Zhang, Y. (2012). GFOLD: a generalized fold change for ranking differentially expressed genes from RNA-seq data. Bioinformatics *28*, 2782–2788.

Foell, D., Frosch, M., Sorg, C., and Roth, J. (2004). Phagocyte-specific calcium-binding S100 proteins as clinical laboratory markers of inflammation. Clin. Chim. Acta *344*, 37–51.

Frieman, M.B., Chen, J., Morrison, T.E., Whitmore, A., Funkhouser, W., Ward, J.M., Lamirande, E.W., Roberts, A., Heise, M., Subbarao, K., and Baric, R.S. (2010). SARS-CoV pathogenesis is regulated by a STAT1 dependent but a type I, II and III interferon receptor independent mechanism. PLoS Pathog. *6*, e1000849.

Giri, K., Pabelick, C.M., Mukherjee, P., and Prakash, Y.S. (2016). Hepatoma derived growth factor (HDGF) dynamics in ovarian cancer cells. Apoptosis *21*, 329–339.

Hadjadj, J., Yatim, N., Barnabei, L., Corneau, A., Boussier, J., Smith, N., Péré, H., Charbit, B., Bondet, V., Chenevier-Gobeaux, C., et al. (2020). Impaired type I interferon activity and inflammatory responses in severe COVID-19 patients. Science *369*, 718–724.

Hanifehnezhad, A., Kehribar, E.S., Öztop, S., Sheraz, A., Kasırga, S., Ergünay, K., Önder, S., Yılmaz, E., Engin, D., Oğuzoğlu, T.C., et al. (2020). Characterization of local SARS-CoV-2 isolates and pathogenicity in IFNAR$^{-/-}$ mice. Heliyon *6*, e05116.

Huang, C., Wang, Y., Li, X., Ren, L., Zhao, J., Hu, Y., Zhang, L., Fan, G., Xu, J., Gu, X., et al. (2020). Clinical features of patients infected with 2019 novel coronavirus in Wuhan, China. Lancet *395*, 497–506.

Kang, R., Chen, R., Zhang, Q., Hou, W., Wu, S., Cao, L., Huang, J., Yu, Y., Fan, X.G., Yan, Z., et al. (2014). HMGB1 in health and disease. Mol. Aspects Med. *40*, 1–116.

Kuri-Cervantes, L., Pampena, M.B., Meng, W., Rosenfeld, A.M., Ittner, C.A.G., Weisman, A.R., Agyekum, R.S., Mathew, D., Baxter, A.E., Vella, L.A., et al. (2020). Comprehensive mapping of immune perturbations associated with severe COVID-19. Sci. Immunol. *5*, eabd7114.

Li, Y., Karlin, A., Loike, J.D., and Silverstein, S.C. (2002). A critical concentration of neutrophils is required for effective bacterial killing in suspension. Proc. Natl. Acad. Sci. USA *99*, 8289–8294.

Li, Y., Chen, M., Cao, H., Zhu, Y., Zheng, J., and Zhou, H. (2013). Extraordinary GU-rich single-strand RNA identified from SARS coronavirus contributes an excessive innate immune response. Microbes Infect. *15*, 88–95.

Li, S.W., Wang, C.Y., Jou, Y.J., Huang, S.H., Hsiao, L.H., Wan, L., Lin, Y.J., Kung, S.H., and Lin, C.W. (2016). SARS Coronavirus Papain-Like Protease Inhibits the TLR7 Signaling Pathway through Removing Lys63-Linked Polyubiquitination of TRAF3 and TRAF6. Int. J. Mol. Sci. *17*, E678.

Liao, Y., Smyth, G.K., and Shi, W. (2019). The R package Rsubread is easier, faster, cheaper and better for alignment and quantification of RNA sequencing reads. Nucleic Acids Res. *47*, e47.

Liao, M., Liu, Y., Yuan, J., Wen, Y., Xu, G., Zhao, J., Cheng, L., Li, J., Wang, X., Wang, F., et al. (2020). Single-cell landscape of bronchoalveolar immune cells in patients with COVID-19. Nat. Med. *26*, 842–844.

Matsuyama, T., Kubli, S.P., Yoshinaga, S.K., Pfeffer, K., and Mak, T.W. (2020). An aberrant STAT pathway is central to COVID-19. Cell Death Differ. *27*, 3209–3225, https://doi.org/10.1038/s41418-020-00633-7.

Meng, H., Yalavarthi, S., Kanthi, Y., Mazza, L.F., Elfline, M.A., Luke, C.E., Pinsky, D.J., Henke, P.K., and Knight, J.S. (2017). In Vivo Role of Neutrophil Extracellular Traps in Antiphospholipid Antibody-Mediated Venous Thrombosis. Arthritis Rheumatol. *69*, 655–667.

Müller, I., Vogl, T., Pappritz, K., Miteva, K., Savvatis, K., Rohde, D., Most, P., Lassner, D., Pieske, B., Kühl, U., et al. (2017). Pathogenic Role of the Damage-Associated Molecular Patterns S100A8 and S100A9 in Coxsackievirus B3-Induced Myocarditis. Circ. Heart Fail. *10*, e004125.

Nagareddy, P.R., Murphy, A.J., Stirzaker, R.A., Hu, Y., Yu, S., Miller, R.G., Ramkhelawon, B., Distel, E., Westerterp, M., Huang, L.S., et al. (2013). Hyperglycemia promotes myelopoiesis and impairs the resolution of atherosclerosis. Cell Metab. *17*, 695–708.

Narumi, K., Miyakawa, R., Ueda, R., Hashimoto, H., Yamamoto, Y., Yoshida, T., and Aoki, K. (2015). Proinflammatory Proteins S100A8/S100A9 Activate NK Cells via Interaction with RAGE. J. Immunol. *194*, 5539–5548.

Nathan, C. (2002). Points of control in inflammation. Nature *420*, 846–852.

Nauseef, W.M., and Borregaard, N. (2014). Neutrophils at work. Nat. Immunol. *15*, 602–611.

Nicolás-Ávila, J.A., Adrover, J.M., and Hidalgo, A. (2017). Neutrophils in Homeostasis, Immunity, and Cancer. Immunity *46*, 15–28.

Ometto, F., Friso, L., Astorri, D., Botsios, C., Raffeiner, B., Punzi, L., and Doria, A. (2017). Calprotectin in rheumatic diseases. Exp. Biol. Med. (Maywood) *242*, 859–873.

Oppenheim, J.J., and Yang, D. (2005). Alarmins: chemotactic activators of immune responses. Curr. Opin. Immunol. *17*, 359–365.

Patel, S. (2018). Danger-Associated Molecular Patterns (DAMPs): the Derivatives and Triggers of Inflammation. Curr. Allergy Asthma Rep. *18*, 63.

Schelbergen, R.F., Geven, E.J., van den Bosch, M.H., Eriksson, H., Leanderson, T., Vogl, T., Roth, J., van de Loo, F.A., Koenders, M.I., van der Kraan, P.M., et al. (2015). Prophylactic treatment with S100A9 inhibitor paquinimod reduces pathology in experimental collagenase-induced osteoarthritis. Ann. Rheum. Dis. *74*, 2254–2258.

Schulte-Schrepping, J., Reusch, N., Paclik, D., Baßler, K., Schlickeiser, S., Zhang, B., Krämer, B., Krammer, T., Brumhard, S., Bonaguro, L., et al.; Deutsche COVID-19 OMICS Initiative (DeCOI) (2020). Severe COVID-19 Is Marked by a Dysregulated Myeloid Cell Compartment. Cell *182*, 1419–1440.e23, e1423.

Shi, H., Zuo, Y., Yalavarthi, S., Gockman, K., Zuo, M., Madison, J.A., Blair, C., Woodward, W., Lezak, S.P., Lugogo, N.L., et al. (2020). Neutrophil calprotectin identifies severe pulmonary disease in COVID-19. J. Leukoc. Biol. https://doi.org/10.1002/JLB.3COVCRA0720-359R.

Silvin, A., Chapuis, N., Dunsmore, G., Goubet, A.G., Dubuisson, A., Derosa, L., Almire, C., Hénon, C., Kosmider, O., Droin, N., et al. (2020). Elevated Calprotectin and Abnormal Myeloid Cell Subsets Discriminate Severe from Mild COVID-19. Cell *182*, 1401–1418.e18, e1418.

Tan, L., Wang, Q., Zhang, D., Ding, J., Huang, Q., Tang, Y.Q., Wang, Q., and Miao, H. (2020). Lymphopenia predicts disease severity of COVID-19: a descriptive and predictive study. Signal Transduct. Target. Ther. *5*, 33.

Totura, A.L., Whitmore, A., Agnihothram, S., Schäfer, A., Katze, M.G., Heise, M.T., and Baric, R.S. (2015). Toll-Like Receptor 3 Signaling via TRIF Contributes to a Protective Innate Immune Response to Severe Acute Respiratory Syndrome Coronavirus Infection. MBio *6*, e00638-15.

Vogl, T., Tenbrock, K., Ludwig, S., Leukert, N., Ehrhardt, C., van Zoelen, M.A., Nacken, W., Foell, D., van der Poll, T., Sorg, C., and Roth, J. (2007). Mrp8 and Mrp14 are endogenous activators of Toll-like receptor 4, promoting lethal, endotoxin-induced shock. Nat. Med. *13*, 1042–1049.

Wang, H., Liao, H., Ochani, M., Justiniani, M., Lin, X., Yang, L., Al-Abed, Y., Wang, H., Metz, C., Miller, E.J., et al. (2004). Cholinergic agonists inhibit HMGB1 release and improve survival in experimental sepsis. Nat. Med. *10*, 1216–1221.

Wang, S., Song, R., Wang, Z., Jing, Z., Wang, S., and Ma, J. (2018). S100A8/A9 in Inflammation. Front. Immunol. *9*, 1298.

Wilk, A.J., Rustagi, A., Zhao, N.Q., Roque, J., Martínez-Colón, G.J., McKechnie, J.L., Ivison, G.T., Ranganath, T., Vergara, R., Hollis, T., et al. (2020). A single-cell atlas of the peripheral immune response in patients with severe COVID-19. Nat. Med. *26*, 1070–1076.

Wu, C., Chen, X., Cai, Y., Xia, J., Zhou, X., Xu, S., Huang, H., Zhang, L., Zhou, X., Du, C., et al. (2020a). Risk Factors Associated With Acute Respiratory Distress Syndrome and Death in Patients With Coronavirus Disease 2019 Pneumonia in Wuhan, China. JAMA Intern. Med. *180*, 934–943, https://doi.org/10.1001/jamainternmed.2020.0994.

Wu, F., Zhao, S., Yu, B., Chen, Y.M., Wang, W., Song, Z.G., Hu, Y., Tao, Z.W., Tian, J.H., Pei, Y.Y., et al. (2020b). A new coronavirus associated with human respiratory disease in China. Nature *579*, 265–269.

Xie, X., Shi, Q., Wu, P., Zhang, X., Kambara, H., Su, J., Yu, H., Park, S.Y., Guo, R., Ren, Q., et al. (2020). Single-cell transcriptome profiling reveals neutrophil heterogeneity in homeostasis and infection. Nat. Immunol. *21*, 1119–1133, https://doi.org/10.1038/s41590-020-0736-z.

Yadav, V., Chi, L., Zhao, R., Tourdot, B.E., Yalavarthi, S., Jacobs, B.N., Banka, A., Liao, H., Koonse, S., Anyanwu, A.C., et al. (2019). Ectonucleotidase tri(di)phosphohydrolase-1 (ENTPD-1) disrupts inflammasome/interleukin 1β-driven venous thrombosis. J. Clin. Invest. *129*, 2872–2877.

Yang, Z., Du, J., Chen, G., Zhao, J., Yang, X., Su, L., Cheng, G., and Tang, H. (2014). Coronavirus MHV-A59 infects the lung and causes severe pneumonia in C57BL/6 mice. Virol. Sin. *29*, 393–402.

Yang, D., Han, Z., and Oppenheim, J.J. (2017). Alarmins and immunity. Immunol. Rev. *280*, 41–56.

You, F., Wang, P., Yang, L., Yang, G., Zhao, Y.O., Qian, F., Walker, W., Sutton, R., Montgomery, R., Lin, R., et al. (2013). ELF4 is critical for induction of type I interferon and the host antiviral response. Nat. Immunol. *14*, 1237–1246.

Zhang, B., Zhou, X., Qiu, Y., Song, Y., Feng, F., Feng, J., Song, Q., Jia, Q., and Wang, J. (2020). Clinical characteristics of 82 cases of death from COVID-19. PLoS One *15*, e0235458.

Zheng, H.Y., Zhang, M., Yang, C.X., Zhang, N., Wang, X.C., Yang, X.P., Dong, X.Q., and Zheng, Y.T. (2020a). Elevated exhaustion levels and reduced functional diversity of T cells in peripheral blood may predict severe progression in COVID-19 patients. Cell. Mol. Immunol. *17*, 541–543.

Zheng, M., Gao, Y., Wang, G., Song, G., Liu, S., Sun, D., Xu, Y., and Tian, Z. (2020b). Functional exhaustion of antiviral lymphocytes in COVID-19 patients. Cell. Mol. Immunol. *17*, 533–535.

Zhou, P., Liu, Z., Chen, Y., Xiao, Y., Huang, X., and Fan, X.G. (2020). Bacterial and fungal infections in COVID-19 patients: A matter of concern. Infect. Control Hosp. Epidemiol. *41*, 1124–1125.

Zhu, N., Zhang, D., Wang, W., Li, X., Yang, B., Song, J., Zhao, X., Huang, B., Shi, W., Lu, R., et al.; China Novel Coronavirus Investigating and Research Team (2020). A Novel Coronavirus from Patients with Pneumonia in China, 2019. N. Engl. J. Med. *382*, 727–733.

Zornetzer, G.A., Frieman, M.B., Rosenzweig, E., Korth, M.J., Page, C., Baric, R.S., and Katze, M.G. (2010). Transcriptomic analysis reveals a mechanism for a prefibrotic phenotype in STAT1 knockout mice during severe acute respiratory syndrome coronavirus infection. J. Virol. *84*, 11297–11309.

Zuo, Y., Yalavarthi, S., Shi, H., Gockman, K., Zuo, M., Madison, J.A., Blair, C., Weber, A., Barnes, B.J., Egeblad, M., et al. (2020). Neutrophil extracellular traps in COVID-19. JCI Insight *5*, 138999.

STAR★METHODS

KEY RESOURCES TABLE

REAGENT or RESOURCE	SOURCE	IDENTIFIER
Antibodies		
Rabbit monoclonal anti-S100A8	Cell Signaling Technology	Cat#47310T
Rat monoclonal anti-CD16/CD32	Thermo Fisher Scientific	Cat#14-0161-82; RRID: AB_467133
Ly-6G Monoclonal Antibody (1A8-Ly6g), APC	Thermo Fisher Scientific	Cat#17-9668-80; RRID: AB_2573306
CD45 Monoclonal Antibody (30-F11), PE	Thermo Fisher Scientific	Cat#12-0451-81; RRID: AB_465667
CD11b Monoclonal Antibody (M1/70), FITC	Thermo Fisher Scientific	Cat#11-0112-81, RRID: AB_464934
Bacterial and virus strains		
IAV (Influenza A Virus, PR8)	Feng Qiang (Fudan University)	N/A
HSV-1 (Herpes simplex virus 1)	A. Iwasaki (Yale University)	N/A
EMCV (Encephalomyocarditis virus)	ATCC	ATCC VR-129B
SARS-CoV-2 (WH-09)	This paper	No. MT093631.2
MHV-A59 (mouse hepatitis virus A-59)	ATCC	ATCC VR-764
Chemicals, peptides, and recombinant proteins		
DMEM Medium	GIBCO	Cat#11965092
Fetal Bovine Serum	PAN	Cat#ST30-3306
DPBS	GIBCO	Cat#14190250
Trypsin	MACGENE	Cat#CC012.1
Penicillin-Streptomycin	MACGENE	Cat#CC004
RPMI 1640 Medium	GIBCO	Cat#22400105
Paquinimod	TargetMol	Cat#T7310
Resatorvid	MCE	Cat#HY-11109
Azeliragon	TargetMol	Cat#T2507
DMSO	VWR	Cat#VWRC0231
Corn oil	MCE	Cat#HY-Y1888
Lipopolysaccharide (LPS)	Sigma-Aldrich	Cat#L4391
TRNzol reagent	Beijing TIANGEN Biotech	Cat#DP424
SYBR qPCR Master mix	Nanjing Vazyme Biotech	Cat#Q331-02
Collagenase D	Sigma-Aldrich	Cat#11088858001
DNase I	STEMCELL Technologies	Cat#07469
Red blood cell lysis buffer	Beijing Solarbio Science & Technology	Cat#R1010
TRNzol reagent	Beijing TIANGEN Biotech	Cat#DP424
Critical commercial assays		
HiScript III 1st Strand cDNA Synthesis Kit	Nanjing Vazyme Biotech	Cat#R312-02
Two-step detection kit	Beijing ZSGB Biotechnology	Cat#PV-9001
Deposited data		
Raw data files for RNA-sequencing	Gene Expression Omnibus	GSE158297
Experimental models: cell lines		
Raw 264.7 cells	ATCC	ATCC TIB-71
17CL-1 cells	Dan L. (Peking University)	N/A
A549 cells	ATCC	ATCC CCL-185
Vero cells	ATCC	ATCC CCL-81
Experimental models: organisms/strains		
Ifnar$^{-/-}$ mice	Erol Fikrig (Yale University)	N/A
Irf3/7$^{-/-}$ mice	Zhengfan J. (Peking University)	N/A
hACE2 mice	This paper	N/A

(*Continued on next page*)

Continued

REAGENT or RESOURCE	SOURCE	IDENTIFIER
Oligonucleotides		
Please refer to Table S1 for details	This paper	N/A
Software and algorithms		
GraphPad Prism 8.0	GraphPad Software	https://www.graphpad.com/scientific-software/prism/; RRID: SCR_002798
FlowJo Software (version 10.7.1)	FlowJo, LLC	https://www.flowjo.com/solutions/flowjo/downloads; RRID: SCR_008520
FastQC v0.11.9	Babraham Institude	http://www.bioinformatics.babraham.ac.uk/projects/fastqc/
Trim Galore v0.6.5	Babraham Institude	http://www.bioinformatics.babraham.ac.uk/projects/trim_galore/
GFOLD v1.1.4	Feng et al., 2012	https://zhanglab.tongji.edu.cn/softwares/GFOLD/index.html
Rsubread v2.4.2	Liao et al., 2019	http://bioconductor.org/packages/Rsubread

RESOURCE AVAILABILITY

Lead contact

Further information and requests for resources and reagents should be directed to and will be fulfilled by the Lead Contact, Fuping You (fupingyou@hsc.pku.edu.cn).

Materials availability

This study did not generate new unique reagents.

Data and code availability

The datasets generated during this study are available at Gene Expression Omnibus (https://www.ncbi.nlm.nih.gov/geo/). The accession number for the original RNA-Seq data reported in this paper is GEO: GSE158297.

EXPERIMENTAL MODEL AND SUBJECT DETAILS

Cells

Raw 274.7 cells, 17CL-1 cells, A549 cells and Vero cells were kept in our lab. Raw 274.7 cells and A549 cells were cultured in RPMI 1640 medium (GIBCO) supplemented with 10% FBS, 100 U/mL Penicillin-Streptomycin. 17CL-1 cells and Vero cells were cultured in DMEM medium (GIBCO) supplemented with 10% FBS (PAN), 100 U/mL Penicillin-Streptomycin. All cells were incubated at 37°C, 5% CO2.

Viruses

A stock of the SARS-CoV-2 virus (WH-09/human/2020/CHN, accession number MT093631.2) was used in this study. IAV (Influenza a Virus, PR8) was a gift from Feng Qiang (Fudan University) and HSV-1 (Herpes simplex virus 1) was from A. Iwasaki (Yale University). EMCV (Encephalomyocarditis virus, VR-129B) was purchased from American Type Culture Collection (ATCC). MHV-A59 (mouse hepatitis virus A-59) has been described previously and was kept in our lab (Yang et al., 2014).

Seed SARS-CoV-2 stocks and virus isolation studies were performed in Vero E6 cells, and the virus titer were determined using a standard TCID50 assay.

IAV was propagated in 10-day-old specific-pathogen-free embryonic chicken eggs. The allantoic fluid was collected and titrated to determine the TCID50 in A549 cells.

EMCV, HSV-1 were propagated in Vero cells, and the supernatants were used as a stock solution. The titer of viruses was determined by plaque assay in Vero cells.

MHV-A59 were propagated in 17CL-1 cells, and the supernatants were used as a stock solution. The titer of the virus was determined by plaque assay in 17CL-1 cells.

Animal experiments

All experiments with live SARS-CoV-2 viruses were carried out in the enhanced biosafety level 3 (P3+) facilities in the Institute of Laboratory Animal Science, Chinese Academy of Medical Sciences (CAMS) approved by the National Health Commission of the People's Republic of China. All animals care and use were in accordance with the Guide for the Care and Use of Laboratory Animals

of the Chinese Association for Laboratory Animal Science. All procedures of animal handling were approved by the Animal Care Committee of Peking University Health Science Center.

All animals were kept and bred in specific pathogen-free conditions under controlled temperature (23 ± 1°C) and exposed to a constant 12 h light-dark cycle. All animals are guaranteed adequate clean water and nutritious feed. Rhesus macaques used in this study were provided by the Institute of Laboratory Animal Science, Chinese Academy of Medical Science. Wild-type (WT) C57BL/6 mice were purchased from Department of Laboratory Animal Science of Peking University Health Science Center, Beijing. The *hACE2* transgenic mice, which were generated by microinjection of the mouse Ace2 promoter driving the human ACE2 coding sequence into the pronuclei of fertilized ova from ICR mice (Bao et al., 2020), were obtained from the Institute of Laboratory Animal Science, Peking Union Medical College. Interferon-α receptor gene knockout (*Ifnar*$^{-/-}$) mice is a gift from Pro. Erol Fikrig (Yale University). *Irf3/7* double knockout mice is a gift from Pro. Zhengfan Jiang (Peking University). Before the experimental operation, all animals are test or drug naive without involvement in any previous procedures. They are healthy and have normal immunity.

METHOD DETAILS

Animal infection assays

For animal infection assay, rhesus macaques (3-4 years old) were anaesthetized with 10 mg/kg ketamine hydrochloride and challenged with 10^6 TCID50 SARS-CoV-2 virus by intratracheal routes. The hACE2 mice were intraperitoneally anaesthetized by 2.5% avertin with 0.02 mL/g body weight and inoculated intranasally with SARS-CoV-2 virus at a dosage of 10^5 TCID50. WT C57BL/6J mice and *Ifnar*$^{-/-}$ mice were anaesthetized by isoflurane. All the mice used were adults aged 6-12 weeks. Age-matched mice were used in the same experiment. IAV is inoculated intranasally at a dosage of 10^5 TCID50. The doses of other inoculated viruses: EMCV (10^7 PFU), HSV-1 (10^6 PFU), MHV-A59 (10^5 PFU). The animals intranasally inoculated with an equal volume of PBS were used as a mock control. The health status and weight of all mice were observed and recorded daily. Rhesus macaques were euthanized at 0, 3- and 5-days post infection (dpi) to collect different tissues and examined virus replication and histopathological changes. Mice were euthanized at 0, 1, 3, 5 and 7 dpi to collect different tissues and examined virus replication and histopathological changes. All the mice depicted in the study are female. However, through observation, we found that male mice seem to die more quickly than female mice after MHV-A59 infection, which may be related to hormonal metabolism between males and females.

RNA sequencing (RNA-seq)

Whole RNA of tissues with specific treatment were purified using TRNzol reagent. The transcriptome library for sequencing was generated using VAHTSTM mRNA-seq v2 Library Prep Kit for Illumina® (Vazyme Biotech Co.,Ltd, Nanjing, China) following the manufacturer's recommendations. After clustering, the libraries were sequenced on Illumina Hiseq X Ten platform using (2 × 150 bp) paired-end module. The raw data were transformed into raw reads by base calling using CASAVA.

Quantitative RT-PCR (qRT-PCR) analysis

Total RNA was isolated from the tissues by TRNzol reagent (DP424, Beijing TIANGEN Biotech, China). Then, cDNA was prepared using HiScript III 1st Strand cDNA Synthesis Kit (R312-02, Nanjing Vazyme Biotech, China). qRT-PCR was performed using the Applied Biosystems 7500 Real-Time PCR Systems (Thermo Fisher Scientific, USA) with SYBR qPCR Master mix (Q331-02, Nanjing Vazyme Biotech, China). The data of qRT-PCR were analyzed by the Livak method ($2^{-\Delta\Delta Ct}$). Ribosomal protein L19 (RPL19) was used as a reference gene for mice, and GAPDH for macaques. The *E* gene of SARS-CoV-2, *N* gene of MHV-A59 and *M1* gene of IAV are examined for quantitation. All gene primers are displayed in supplementary materials Table S1.

Histology and immunohistochemical staining

The lungs were quickly placed in cold saline solution and rinsed after they were collected. Then, lungs were fixed in 4% paraformaldehyde, dehydrated and embedded in paraffin prior to sectioning at 5 μm, and sections were stained with hematoxylin and eosin. Several pulmonary H&E staining images were randomly selected for pathological scoring in a blinded fashion. Lung damage is classified into five levels by pathological scoring. "0" represents no abnormality, "1" represents very small pathological changes, "2" represents slight pathological changes, "3" represents moderate pathological changes and "4" represents serious pathological changes.

For immunohistochemical staining, the lung paraffin sections were dewaxed and rehydrated through xylene and an alcohol gradient. Antigen retrieval was performed by heating the sections to 100°C for 4 min in 0.01 M citrate buffer (pH 6.0) and repeated 4 times. The operations were performed according to the instructions of the two-step detection kit (PV-9001, Beijing ZSGB Biotechnology, China). The samples were treated by endogenous peroxidase blockers for 10 min at room temperature followed by incubation with primary antibodies S100A8 (1:200, 47310T, Cell Signaling Technology) at 37°C for 1 h, then after washed with PBS. The samples were incubated with reaction enhancer for 20 min at room temperature and secondary antibodies at 37°C for 30 min, and finally sections were visualized by 3,30-diaminobenzidine tetrahydrochloride (DAB) and counterstained with hematoxylin.

Tissue preparation and flow cytometry

The lung tissues, peripheral blood and bone marrow were collected from the mice. The lungs were first ground with 200-mesh copper sieve, and then transferred to DMEM containing 10% FBS, 0.5 mg/mL Collagenase D (11088858001, Roche, Switzerland) and 0.1 mg/mL DNase I (07469, STEMCELL Technologies, Canada) for a 20 min digestion at 37°C to obtain single-cell suspensions. Bone marrow were flushed out of the femurs using a 23–gauge needle in PBS containing 2mM EDTA and 2% fetal bovine serum (FBS) and dispersed into single cells through a pipette. Single-cell samples were treated by red blood cell lysis buffer (R1010, Beijing Solarbio Science & Technology, China) for 2 min at room temperature and passed through a 200-mesh copper sieve before staining. Peripheral blood was treated with red blood cell lysis buffer to remove red blood cells.

After blocking non-specific Fc receptor-mediated interactions with CD16/CD32 antibodies (14-0161-82, eBioscience, USA), single-cell suspensions were stained with fluorophore-conjugated anti-mouse antibodies at 4°C for 30min. After washing the samples, flow cytometry acquisition was performed on a BD LSRFortessa. Sorting were performed using a BD AriaIII (BD). All antibodies were purchased from eBioscience: CD45-PE (12-0451-81), Ly-6G-APC (17-9668-80), and CD11b-FITC (11-0112-81).

Drug rescue assay

For the Paquinimod rescue assay, all mice were challenged by viruses and randomly divided into two groups, in which one group was given intranasally 12.5 μg/day of Paquinimod (TargetMol; Catalog No. T7310) starting on 2 dpi and the other group was treated with equal volume PBS as the control group. Stock solutions of 100 mg/mL Paquinimod were prepared with DMSO in advance. The health status and weight of all mice were observed and recorded daily.

For the Resatorvid/Azeliragon rescue assay, the mice challenged by viruses were given intraperitoneally 50 μg/day of Resatorvid (MCE; Synonyms: TAK-242; CLI-095) and 100 μg/day of Azeliragon (TargetMol; Catalog No. T2507) starting on 2 dpi. Stock solutions of 10 mM Resatorvid and 10 mM Azeliragon were prepared with DMSO in advance and was diluted by corn oil. The control group mice were given intraperitoneally 200 μL of corn oil solution which contained 20 μL of DMSO. The health status and body weight of all mice were observed and recorded daily.

Cell co-culture assay

Raw 264.7 cells were seeded on 6-well plates with 10^6 cells/mL. After cell adherence, LPS (100 ng/mL) and mS100A8/A9 protein (1 μM) with or without Resatorvid (100 nM) were added. After 12 h co-culture, cells were harvested and lysed by TRNzol reagent for RNA extraction. Then, the expression of related genes was detected by qRT-PCR.

QUANTIFICATION AND STATISTICAL ANALYSIS

RNA-seq analysis

The FastQC and Trim Galore were used for raw data quality control, then the R package Rsubread was used for mapping and counting the reads. The count matrix was normalized by FPKM. The differentially expressed genes were identified by the GFOLD, a Linux software. The GO and KEGG annotations of DEGs were performed in the DAVID database (https://david.ncifcrf.gov/home.jsp).

Data analysis for flow cytometry data

Flow cytometry data analysis was performed with FlowJo V10.0.7. Relative cell percentage was used for visualization.

Statistical analysis

All analyses were repeated at least three times, and a representative experimental result was presented. Prism 8 software (Graphic software) was used for survival curves, charts and statistical analyses. Two-tailed unpaired Student's t test was used for statistical analysis to determine significant differences when a pair of conditions was compared. Asterisks denote statistical significance (*$p < 0.05$; **$p < 0.01$; ***$p < 0.001$). The data are reported as the mean ± SD. The exact value of n representing number of animals are included in each figure legend.

Cell Host & Microbe, Volume *29*

Supplemental Information

Induction of alarmin S100A8/A9 mediates activation of aberrant neutrophils in the pathogenesis of COVID-19

Qirui Guo, Yingchi Zhao, Junhong Li, Jiangning Liu, Xiuhong Yang, Xuefei Guo, Ming Kuang, Huawei Xia, Zeming Zhang, Lili Cao, Yujie Luo, Linlin Bao, Xiao Wang, Xuemei Wei, Wei Deng, Nan Wang, Luoying Chen, Jingxuan Chen, Hua Zhu, Ran Gao, Chuan Qin, Xiangxi Wang, and Fuping You

Supplemental Information

Figure S1. Antiviral innate immune disorder in the early stage of SARS-CoV-2 infection. (Related to Figure 1)

Figure S2. Analysis of the differences between coronavirus and influenza a virus infection. (Related to Figure 2)

Figure S3. Analysis of immune characteristics of mouse coronavirus MHV-A59 infection. (Related to Figure 2)

Figure S4. Aberrant neutrophils are closely associated with fatal coronavirus infection. (Related to Figure 3)

Figure S5. Analysis of the efficacy of Paquinimod in rescuing mice infected with coronavirus. (Related to Figure 4)

Figure S6. An attempt to treat mice infected with coronavirus via Azeliragon. (Related to Figure 5)

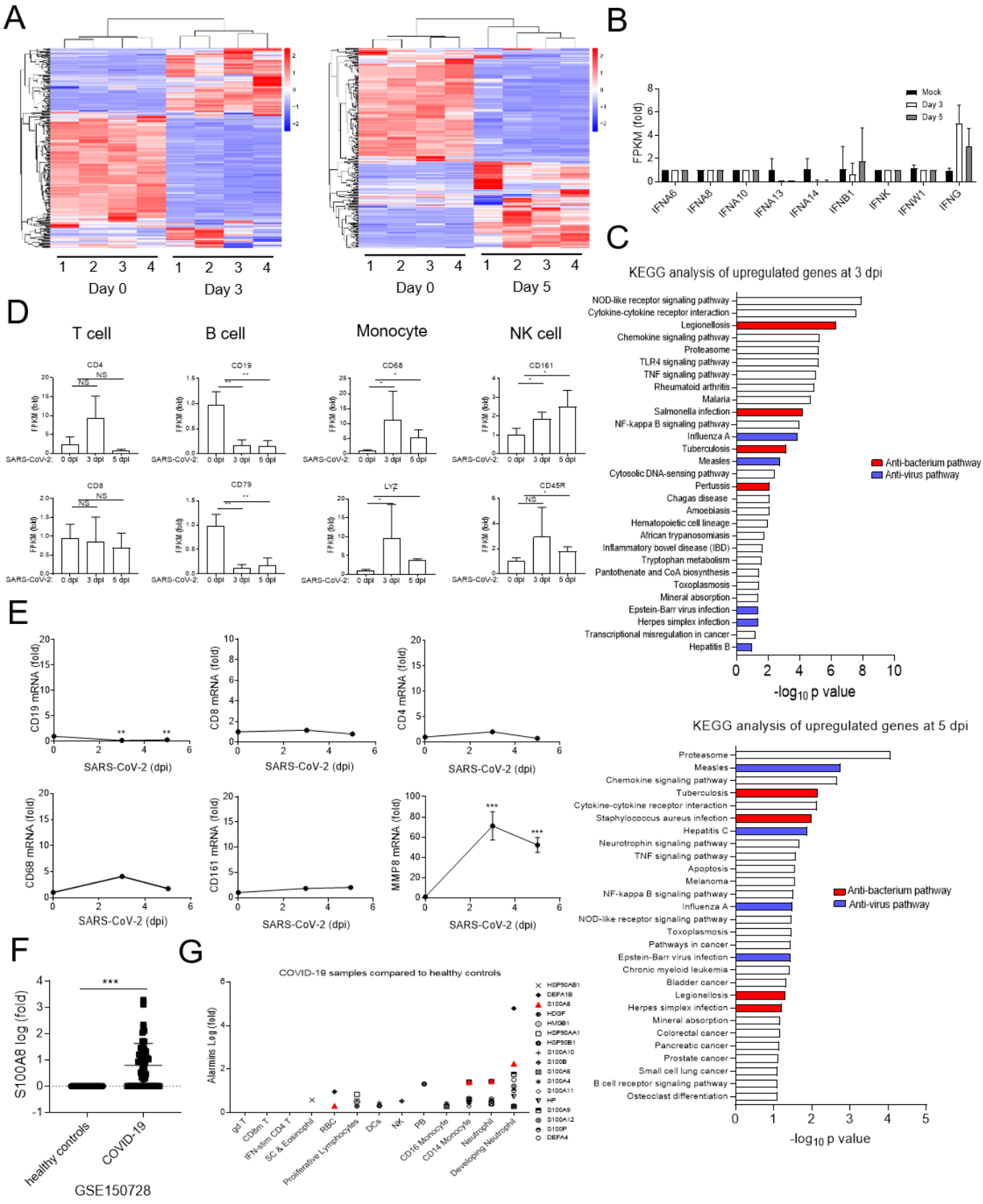

Figure S1. Antiviral innate immune disorder in the early stage of SARS-CoV-2 infection. (Related to Figure 1)

(A) Heat map depicting the differentially expressed genes in the lungs of rhesus macaques infected with SARS-CoV-2 at 3 dpi and 5 dpi. **(B)** The expression of IFNs was analyzed in the lungs of rhesus macaques infected with SARS-CoV-2 at 3 dpi and 5 dpi. **(C)** KEGG analysis of the differences in rhesus macaques infected with SARS-CoV-2 compared with Mock. **(D)** The expression of indicated marker genes was analyzed.

n = 4. **(E)** qRT-PCR analysis of indicated marker genes in the lungs of SARS-CoV-2-infected rhesus macaques at 0 dpi, 3 dpi and 5 dpi. *n=3*. **(F)-(G)** Analysis of *S100A8* (F) and alarmins (G) expression in peripheral blood from healthy control and COVID-19 patients. Fold change (FC) to healthy control (log10). Data from the peripheral blood of COVID-19 patients and healthy control correspond to GEO: GSE150728. (*P < 0.05; **P < 0.01; ***P < 0.001).

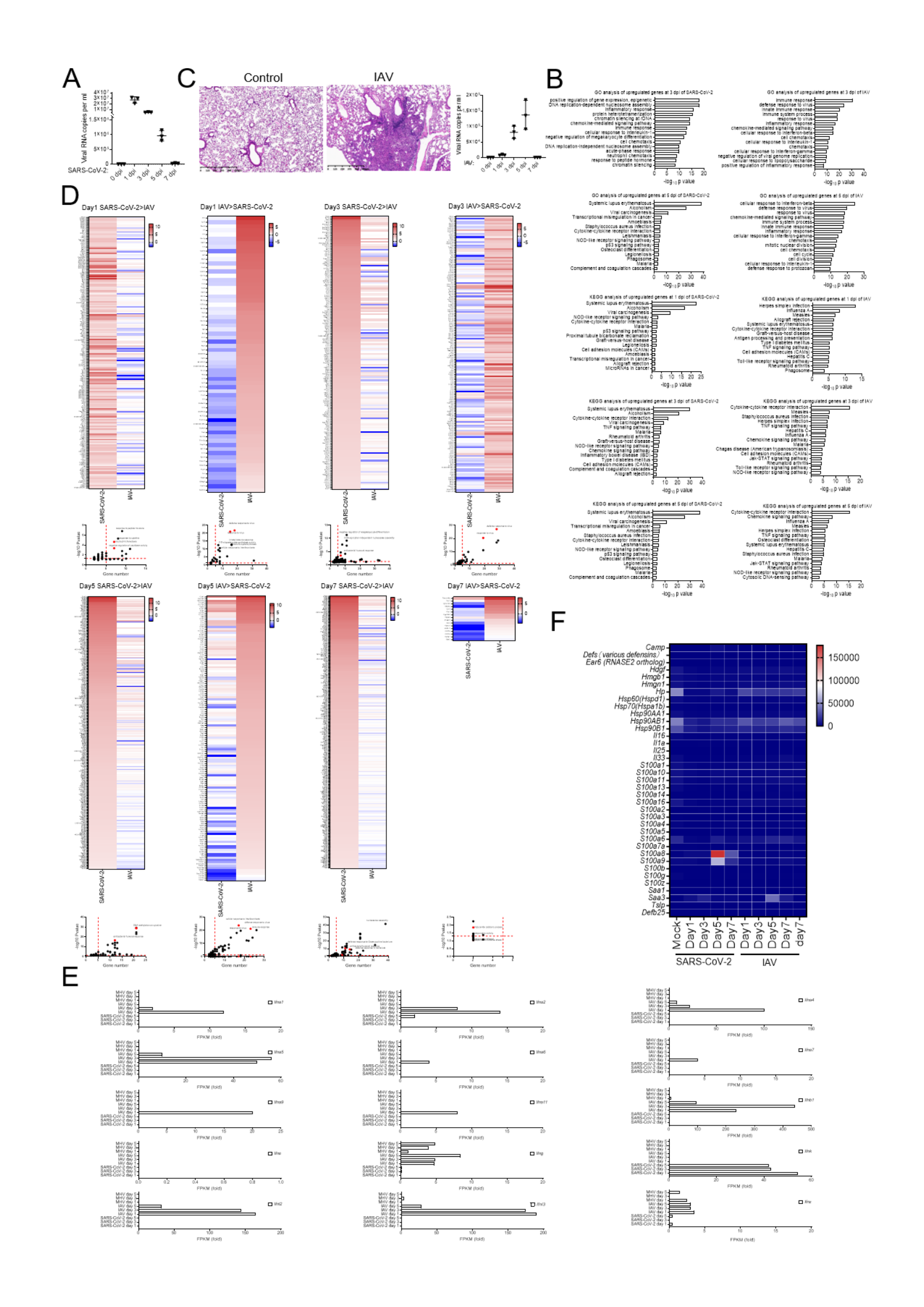
A
Viral RNA copies per ml
SARS-CoV-2:
0 dpi
1 dpi
3 dpi
5 dpi
7 dpi
C
Control
IAV
Viral RNA copies per ml
IAV:
B
GO analysis of upregulated genes at 3 dpi of SARS-CoV-2
GO analysis of upregulated genes at 3 dpi of IAV
GO analysis of upregulated genes at 5 dpi of SARS-CoV-2
GO analysis of upregulated genes at 5 dpi of IAV
KEGG analysis of upregulated genes at 1 dpi of SARS-CoV-2
KEGG analysis of upregulated genes at 1 dpi of IAV
KEGG analysis of upregulated genes at 3 dpi of SARS-CoV-2
KEGG analysis of upregulated genes at 3 dpi of IAV
KEGG analysis of upregulated genes at 5 dpi of SARS-CoV-2
KEGG analysis of upregulated genes at 5 dpi of IAV
-log10 p value
D
Day1 SARS-CoV-2>IAV
Day1 IAV>SARS-CoV-2
Day3 SARS-CoV-2>IAV
Day3 IAV>SARS-CoV-2
Day5 SARS-CoV-2>IAV
Day5 IAV>SARS-CoV-2
Day7 SARS-CoV-2>IAV
Day7 IAV>SARS-CoV-2
SARS-CoV-2
IAV
-log10 Pvalue
Gene number
F
Camp
Defs (various defensins)
Ear6 (RNASE2 ortholog)
Hdgf
Hmgb1
Hmgn1
Hp
Hsp60(Hspd1)
Hsp70(Hspa1b)
Hsp90AA1
Hsp90AB1
Hsp90B1
Il16
Il1a
Il25
Il33
S100a1
S100a10
S100a11
S100a13
S100a14
S100a16
S100a2
S100a3
S100a4
S100a5
S100a6
S100a7a
S100a8
S100a9
S100b
S100g
S100z
Saa1
Saa3
Tslp
Defb25
150000
100000
50000
0
Mock
Day1
Day3
Day5
Day7
Day1
Day3
Day5
Day7
day7
SARS-CoV-2
IAV
E
FPKM (fold)

Figure S2. Analysis of the differences between coronavirus and influenza a virus infection. (Related to Figure 2)

(A) qRT-PCR analysis for viral loads in the lungs of *hACE2* mice infected with SARS-CoV-2. *n=3*. **(B)** RNA-seq analysis of lungs in IAV- and SARS-CoV-2-infected mice at different points in time. GO and KEGG analysis were performed with the differentially expressed genes compared with Mock (*FC > 4 or < 0.25, P value < 0.05*). **(C)** Identification of a mouse model of pneumonia infected with IAV virus. H&E staining of the lung in mice infected with IAV at 5 dpi showed that lots of lymphocytes were infiltrating into the lungs and the lung tissue was obviously fibrotic. qRT-PCR analysis showed that IAV virus amplified effectively in the lung tissue. *n=3*. **(D)** GO and KEGG analysis was performed with the differentially expressed genes between IAV and SARS-CoV-2 infection (*FC > 4 or < 0.25, P value < 0.05*). **(E)** The expression of *IFNs* was analyzed by the RNA-seq data on lungs of mice infected by IAV, MHV or SARS-CoV-2. **(F)** Heat map depicting the expression of alarmins in the lungs of mice infected with IAV and SARS-CoV-2 at successive time points after infection.

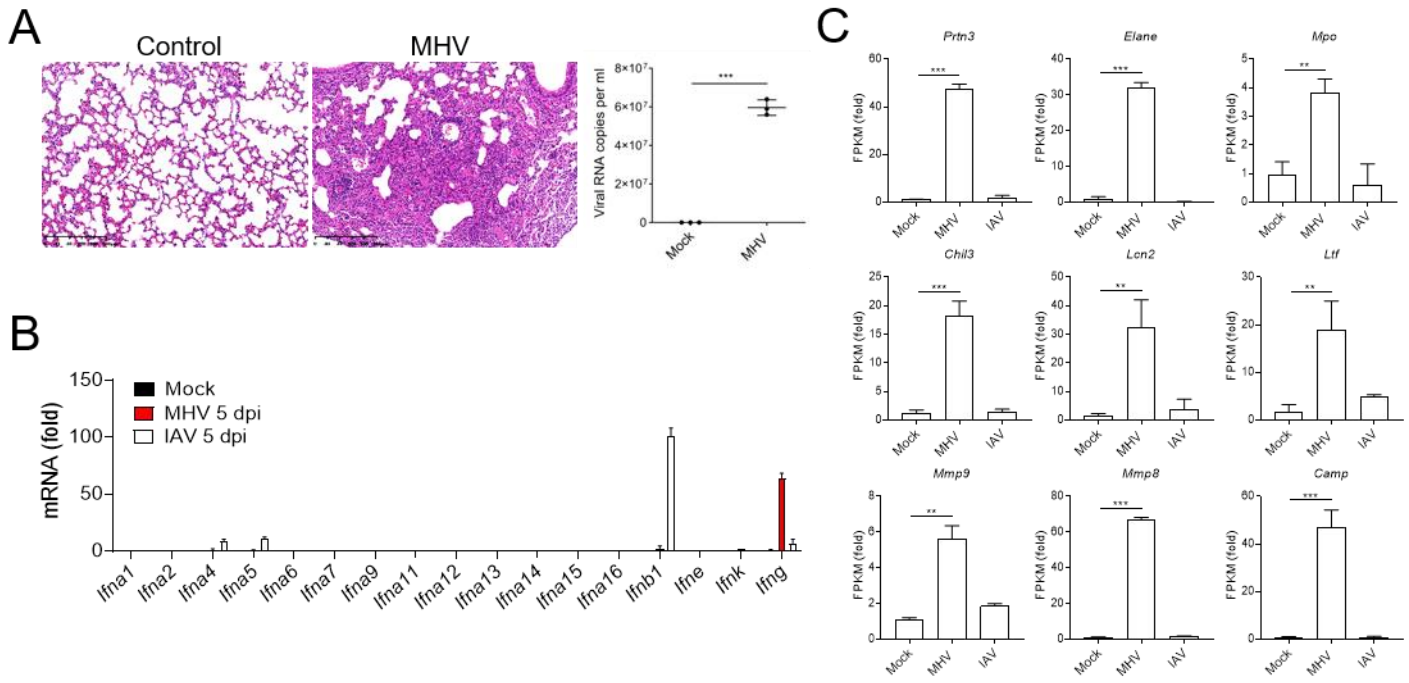

Figure S3. Analysis of immune characteristics of mouse coronavirus MHV-A59 infection. (Related to Figure 2).

(A) Identification of a mouse model of pneumonia infected with MHV virus. H&E staining of the lung in mice infected with MHV at 5 dpi showed significant pulmonary fibrosis. qRT-PCR analysis showed that MHV virus amplified significantly in the lung of mice. *n=3*. **(B)-(C)** The expression of *IFNs* (H) and neutrophil maker genes (I) in the lungs of mice infected with IAV or MHV at 5 dpi were analyzed using RNA-seq data (FC to Mock). (***P < 0.01; ***P < 0.001*).

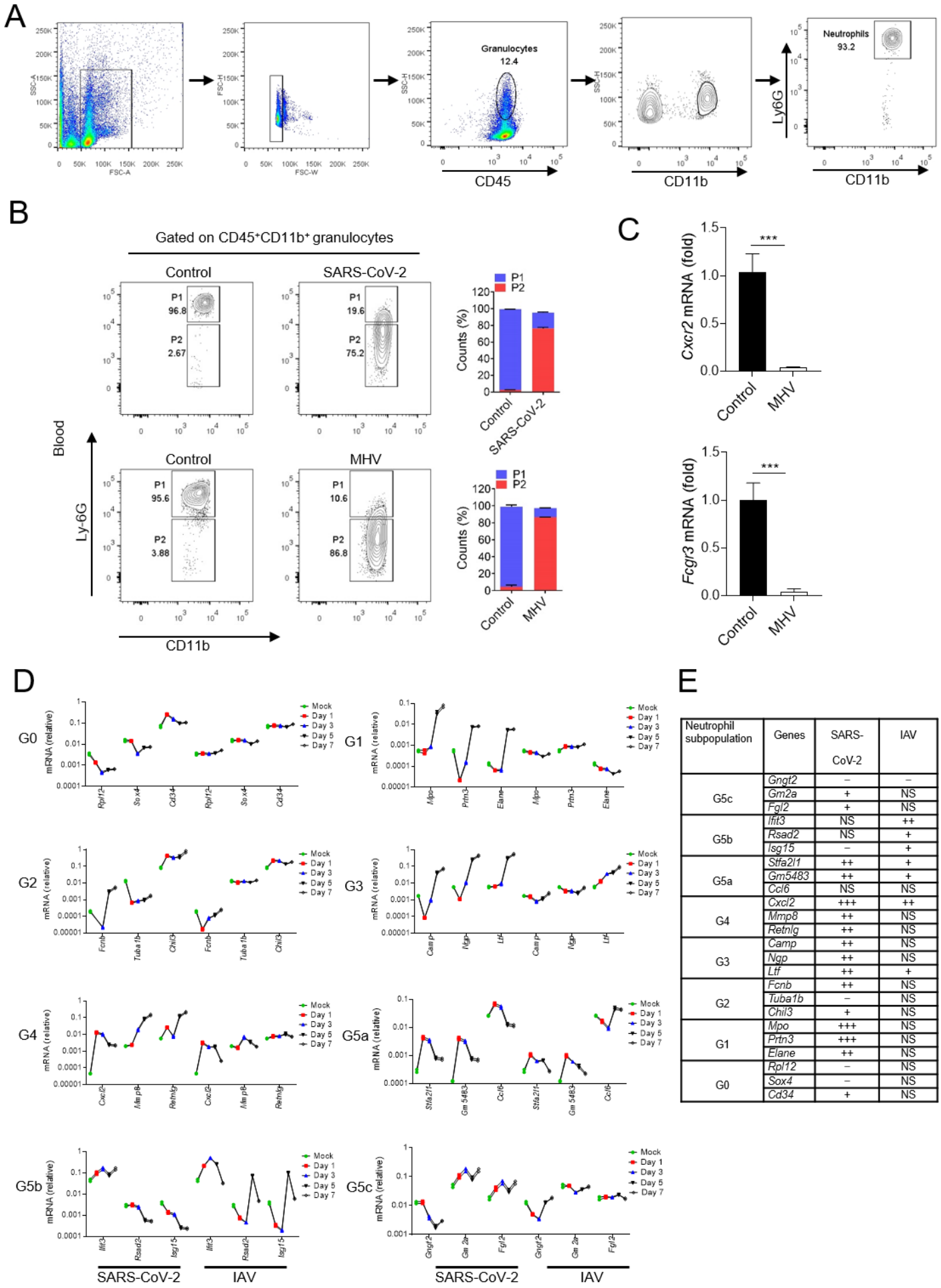

Neutrophil subpopulation	Genes	SARS-CoV-2	IAV
G5c	*Gngt2*	–	–
	Gm2a	+	NS
	Fgl2	+	NS
G5b	*Ifit3*	NS	++
	Rsad2	NS	+
	Isg15	–	+
G5a	*Stfa2l1*	++	+
	Gm5483	++	+
	Ccl6	NS	NS
G4	*Cxcl2*	+++	++
	Mmp8	++	NS
	Retnlg	++	NS
G3	*Camp*	++	NS
	Ngp	++	NS
	Ltf	++	+
G2	*Fcnb*	++	NS
	Tuba1b	–	NS
	Chil3	+	NS
G1	*Mpo*	+++	NS
	Prtn3	+++	NS
	Elane	++	NS
G0	*Rpl12*	–	NS
	Sox4	–	NS
	Cd34	+	NS

Figure S4. Aberrant neutrophils are closely associated with fatal coronavirus infection. (Related to Figure 3)

(A) A flow chart depicting the gating scheme of neutrophils. **(B)** Flow cytometry analysis of neutrophils in blood from mice infected with SARS-CoV-2 and MHV at 5 dpi. Gate P1 shows the conventional neutrophils ($CD45^{+}CD11b^{+}Ly6G^{high}$), and Gate P2 shows the pathologic aberrant neutrophils ($CD45^{+}CD11b^{+}Ly6G^{variable}$). Aberrant neutrophils (P2) in the blood of mice infected with coronavirus were significantly increased. $n = 3$. **(C)** qRT-PCR analysis for the expression of mature neutrophil marker genes *Fcgr3* and *Cxcr2* in aberrant neutrophils of bone marrow. $n = 3$. **(D)-(E)** RNA-seq analysis for related genes of neutrophil differentiation subgroup from the lungs of mice infected with SARS-CoV-2 or IAV. (***$P < 0.001$).

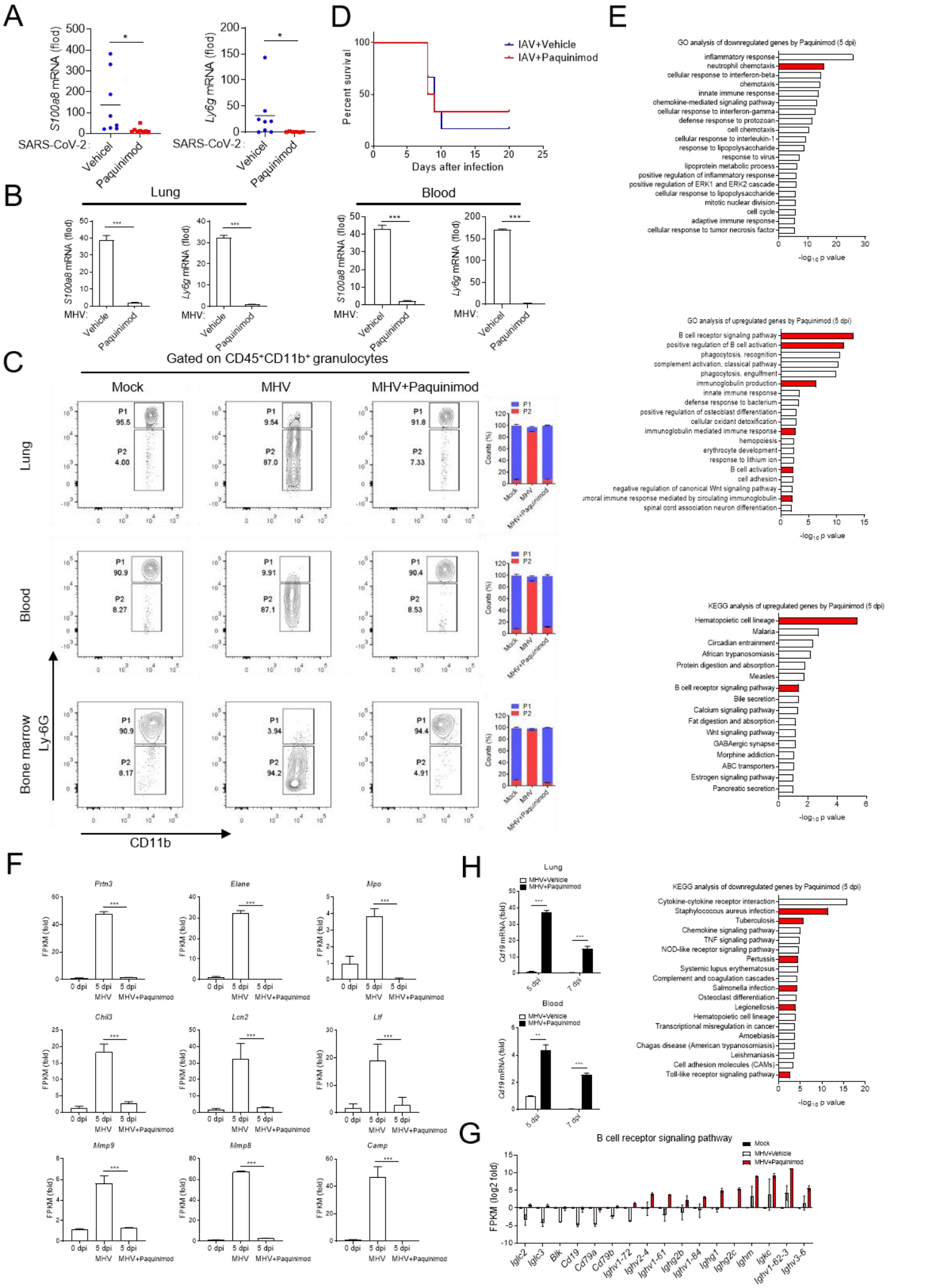
A
S100a8 mRNA (flod)
Ly6g mRNA (flod)
SARS-CoV-2 :
Vehicel
Paquinimod
D
Percent survival
Days after infection
IAV+Vehicle
IAV+Paquinimod
E
GO analysis of downregulated genes by Paquinimod (5 dpi)
inflammatory response
neutrophil chemotaxis
cellular response to interferon-beta
chemotaxis
innate immune response
chemokine-mediated signaling pathway
cellular response to interferon-gamma
defense response to protozoan
cell chemotaxis
cellular response to interleukin-1
response to lipopolysaccharide
response to virus
lipoprotein metabolic process
positive regulation of inflammatory response
positive regulation of ERK1 and ERK2 cascade
cellular response to lipopolysaccharide
mitotic nuclear division
cell cycle
adaptive immune response
cellular response to tumor necrosis factor
-log10 p value
B
Lung
Blood
MHV:
C
Gated on CD45+CD11b+ granulocytes
Mock
MHV
MHV+Paquinimod
Lung
Blood
Bone marrow
Ly-6G
CD11b
P1
P2
Counts (%)
GO analysis of upregulated genes by Paquinimod (5 dpi)
B cell receptor signaling pathway
positive regulation of B cell activation
phagocytosis, recognition
complement activation, classical pathway
phagocytosis, engulfment
immunoglobulin production
innate immune response
defense response to bacterium
positive regulation of osteoblast differentiation
cellular oxidant detoxification
immunoglobulin mediated immune response
hemopoiesis
erythrocyte development
response to lithium ion
B cell activation
cell adhesion
negative regulation of canonical Wnt signaling pathway
humoral immune response mediated by circulating immunoglobulin
spinal cord association neuron differentiation
KEGG analysis of upregulated genes by Paquinimod (5 dpi)
Hematopoietic cell lineage
Malaria
Circadian entrainment
African trypanosomiasis
Protein digestion and absorption
Measles
B cell receptor signaling pathway
Bile secretion
Calcium signaling pathway
Fat digestion and absorption
Wnt signaling pathway
GABAergic synapse
Morphine addiction
ABC transporters
Estrogen signaling pathway
Pancreatic secretion
F
Prtn3
Elane
Mpo
Chil3
Lcn2
Ltf
Mmp9
Mmp8
Camp
FPKM (fold)
0 dpi
5 dpi MHV
5 dpi MHV+Paquinimod
H
Lung
Blood
MHV+Vehicle
MHV+Paquinimod
Cd19 mRNA (fold)
5 dpi
7 dpi
KEGG analysis of downregulated genes by Paquinimod (5 dpi)
Cytokine-cytokine receptor interaction
Staphylococcus aureus infection
Tuberculosis
Chemokine signaling pathway
TNF signaling pathway
NOD-like receptor signaling pathway
Pertussis
Systemic lupus erythematosus
Complement and coagulation cascades
Salmonella infection
Osteoclast differentiation
Legionellosis
Hematopoietic cell lineage
Transcriptional misregulation in cancer
Amoebiasis
Chagas disease (American trypanosomiasis)
Leishmaniasis
Cell adhesion molecules (CAMs)
Toll-like receptor signaling pathway
G
B cell receptor signaling pathway
Mock
MHV+Vehicle
MHV+Paquinimod
FPKM (log2 fold)
Iglc2
Iglc3
Blk
Cd19
Cd79a
Cd79b
Ighv1-72
Ighv2-4
Ighv1-61
Ighg2b
Ighv1-84
Ighg1
Ighg2c
Ighm
Igkc
Ighv1-62-3
Ighv3-6

Figure S5. Analysis of the efficacy of Paquinimod in rescuing mice infected with coronavirus. (Related to Figure 4)

(A) qRT-PCR analysis for the expression of *S100a8* and *Ly6g* in the blood of mice infected with SARS-CoV-2 at 5 dpi after Paquinimod treatment. $n \geq 5$. **(B)** qRT-PCR analysis for the expression of *S100a8* and *Ly6g* in the lungs and blood of mice infected with MHV after Paquinimod treatment. $n = 3$. **(C)** Flow cytometry analysis of neutrophils in lungs, blood and bone marrow from mice infected with MHV at 5 dpi after Paquinimod treatment. Aberrant neutrophils (P2) in the mice infected with MHV were significantly decreased by Paquinimod treatment. $n = 3$. **(D)** Post-infection survival curves of wild type mice infected with IAV by Paquinimod treatment. $n=6$. **(E)** RNA-seq analysis for lungs of MHV-infected *Ifnar*$^{-/-}$ mice rescued by Paquinimod treatment at 5 dpi. GO and KEGG analysis was performed with the differentially expressed genes compared with control ($FC > 4$ *or* < 0.25, *P value* < 0.05). Control group means MHV-infected *Ifnar*$^{-/-}$ mice treated with Vehicle. **(F)** The expression of neutrophil maker genes in the lungs of MHV-infected mice rescued by Paquinimod at 5 dpi were analyzed by RNA-seq data. **(G)-(H)** Analysis of the expression level of B cell related genes in the lungs and blood of MHV-infected mice rescued by Paquinimod. $n = 3$. (*$P < 0.05$; **$P < 0.01$; ***$P < 0.001$).

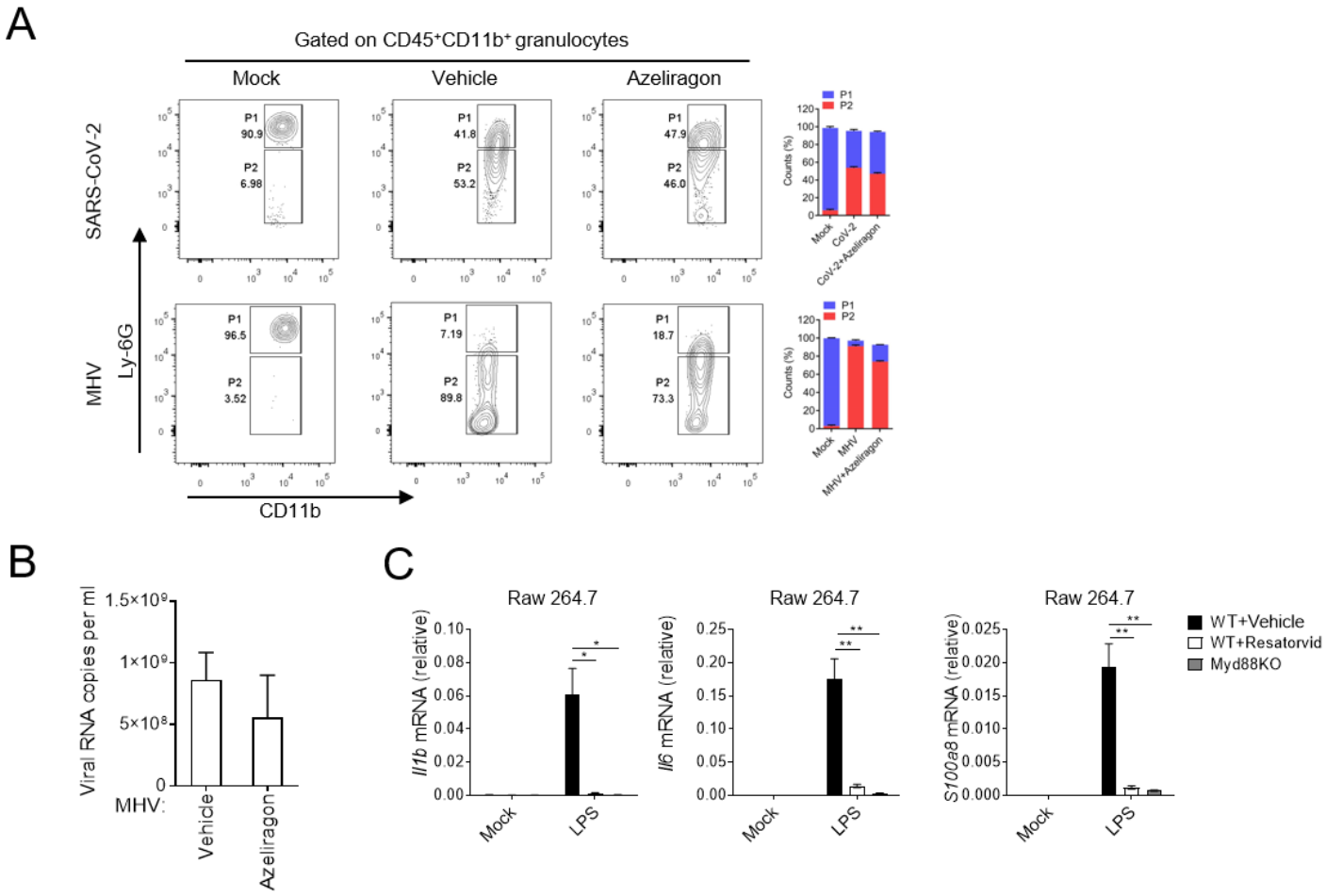

Figure S6. An attempt to treat mice infected with coronavirus via Azeliragon. (Related to Figure 5)

(A) Flow cytometry analysis of neutrophils in the lungs from mice infected with SARS-CoV-2 and MHV at 5 dpi after Azeliragon treatment. *n = 3.* **(B)** Analysis of viral loads in the lungs from MHV-infected mice at 5 dpi after Azeliragon treatment. *n = 3.* **(C)** Identified TLR4 signal response in the Raw 264.7 cells by qRT-PCR. *n = 3.* (*$P < 0.05$; **$P < 0.01$).